Phenoxyamidine Zn and Al Complexes: Synthesis, Characterization, and Use in the Ring-Opening Polymerization of Lactide

Florian Chotard, Rosita Lapenta, Anaëlle Bolley, Audrey Trommenschlager, Cédric Balan, Jérome Bayardon, Raluca Malacea-Kabbara, Quentin Bonnin, Ewen Bodio, Hélène Cattey, et al.

Phenoxyamidine Zn and Al complexes: synthesis, characterization and use in the ROP of Lactide

Florian Chotard,[†] Rosita Lapenta, [§,#] Anaëlle Bolley, [§] Audrey Trommenschlager,[†] Cédric Balan,[†] Jérôme Bayardon,[†] Raluca Malacea-Kabbara,[†] Quentin Bonnin,[†] Ewen Bodio,[†] Hélène Cattey,[†] Philippe Richard,[†] Stefano Milione, [#] Alfonso Grassi,[#] Samuel Dagorne*[§] and Pierre Le Gendre*[†]

[†]Institut de Chimie Moléculaire de l'Université de Bourgogne (ICMUB, UMR-CNRS 6302), Université Bourgogne Franche-Comté

[§]Institut de Chimie de Strasbourg (UMR-CNRS 7177), Université de Strasbourg

Dipartimento di Chimica e Biologia, Universita` degli Studi di Salerno, via Giovanni Paolo II, 132-84084 Fisciano (SA), Italy

Supporting Information

ABSTRACT: Herein we report the synthesis of new ditopic ligands, which consist of a phenoxy group and *N*,*N*,*N'*-trisubstituted amidines linked by a methylene spacer (**L1**-**L4**). Their coordination chemistry has been studied/investigated with Zn(II) and Al(III). Alkane elimination route between the phenol-amidine proligands (**L1H**-**L4H**) and Et_2Zn led to dinuclear complexes [(**L1**-**L4**)ZnEt]$_2$ (**1a**-**4a**) in which the Zn centers are chelated by phenoxyamidine ligands and bridged through the oxygen atom of the phenoxy groups. Salt metathesis reaction between two equivalents of the sodium amidine phenate **L1Na** and $ZnCl_2$ led to a bis-chelate chiral spiro-complex (**L1**$_2$Zn) **1a'**. Analogous alkane elimination route between $AlMe_3$ and the phenol-amidine proligands **L1H**-**L4H** allowed the preparation of the mononuclear complexes [(**L1**-**L4**)$AlMe_2$] (**1b**-**4b)**. The phenoxyamidine-Al and Zn complexes have been characterized by NMR spectroscopy, elemental analysis and/or high resolution ESI-MS. The solid state structures of the proligands **[L1H$_2$][Br]** and **L2H** as well as of six complexes have been established by single crystal X-ray diffraction analysis. Fluxional properties of the proligands **L1H**-**L2H** and of the complexes **1a** and **2b** have been investigated by VT NMR experiments. In the presence of an alcohol source, complexes **1a**-**4a** and **1b**-**4b** were used as initiators for the controlled ring-opening polymerization (ROP) of *rac*-lactide to afford atactic polylactic acid (PLA).

INTRODUCTION

Phenoxyimines (**I**), also known as hemisalen, are among the most versatile ligands in coordination chemistry and afford particularly efficient metal complexes for catalytic purposes (Fig. 1).[1,2,3] These ligands have also found applications in therapy[4] and in preparation of liquid crystalline metal complexes.[5] One advantage of these ligands, beside their ease of access, is the possibility to fine-tune their stereoelectronic properties by introducing different substituents onto the phenoxy ring or at the nitrogen atom of the imine function. Greater alterations of these properties have been brought about by replacing either the phenoxy or the imine moiety by another donor group. As representative examples, thiophenoxyimine (**II**),[6] anilidoimine (**III**),[7] phenoxyamine (**IV**)[8] and phenoxyiminophosphorane (**V**)[9] have been described. The phenoxy moiety has also been combined with a great variety of *N*-heterocycles to furnish ditopic ligands.[10] These variants have proven to be very effective, surpassing in several cases the performances of the original phenoxyimine derivatives. With this in mind, we seek to develop a new class of ligand (**VI**) by replacing the imine function of phenoxyimines with a *N*,*N*,*N'*-trisubstituted amidine. The additional NR'$_2$ group in the amidine moiety with respect to the imine function should make it possible to generate a great diversity of structures, provide additional steric bulk close to the metal center and confer enhanced π-donor ability to the ligand. The methylene spacer as well as the reversed orientation of the imino group (C=N) of the

amidine moiety, compared to phenoxyimine, should allow the formation of a 6-membered chelate ring while preserving the *E*-configuration of the *N,N,N'*-trisubstituted amidine, which is more thermodynamically favorable.[11]

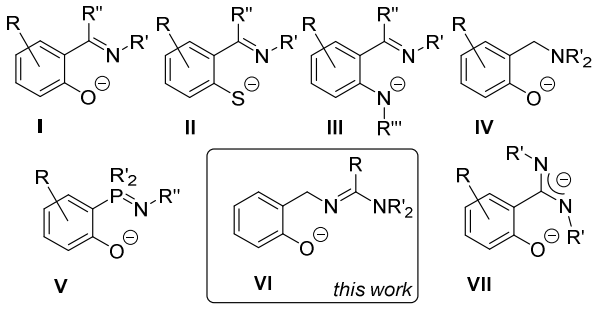

Figure 1. Phenoxyimines (**I**) and related ligands.

One should highlight that the coordination chemistry of *N,N,N'*-trisubstituted amidine remains little explored thus far.[12] This might be explained by the fact that this chemistry is dominated by the negatively charged amidinate ligands for which *N,N,N'*-trisubstituted amidine are *de facto* excluded.[13] Kirillov and Carpentier described previously phenoxy-amidinate ligand (**VII**) and their group 4 and Rare-Earth metal complexes.[14] They also showed that the protonated monoanionic form of this ligand (*i.e.* phenoxyamidine) can coordinate both yttrium and zirconium metal ions, the presence of the NH functionality being *a priori* detrimental to olefin polymerization activity. Herein we report the synthesis of a series of phenoxyamidine ligands (**VI**) bearing a *N,N,N'*-trisubstituted amidine and their coordination chemistry toward zinc(II) and aluminum(III) metal ions. The catalytic activity of these complexes in the ROP of *rac*-lactide was studied and is also reported herein.[15]

RESULTS AND DISCUSSION

Synthesis of ligands and complexes. The phenol-amidine proligands **L1H-L4H** were prepared by two different methods depending on the amidine-carbon substituent (Scheme 1).[16]

Scheme 1. Synthesis of the phenol-amidine proligands[a]

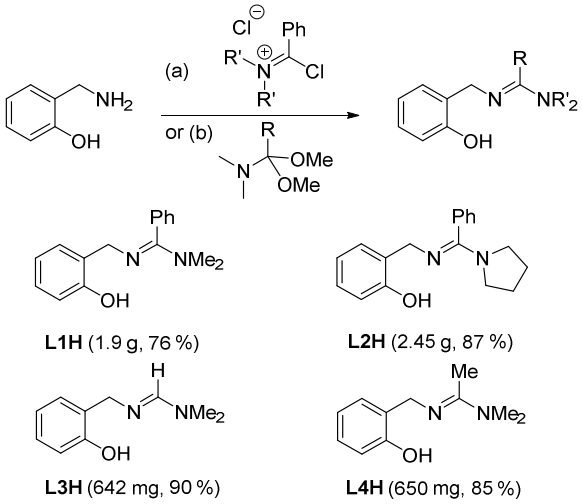

[a]Reagents and conditions: (a) NEt_3 (5 equiv.), DCM, 0 °C to r.t., 16 h; (b) DCM, MW, 50 °C, 10 min.

For the benzamidine proligands **L1H** and **L2H** (method a), Vilsmeier-type reagents were prepared from oxalyl chloride and suitable amide. The resulting chlorobenziminium chloride salts were next reacted with 2-hydroxybenzylamine in the presence of 5 equiv. of triethylamine in dichloromethane to afford **L1H** and **L2H** proligands with good yield on a (multi)gram scale. A ^{1}H NMR stability study revealed that **L1H** is not stable in CD_2Cl_2 and leads to the formation of 2-phenyl-4H-3,1-benzoxazine and dimethylamine (Fig. S9, SI). This intramolecular ring-closing reaction is however rather slow and reaches 90% conversion after 15 days. The phenol-formamidine and -acetamidine proligands **L3H** and **L4H** (method b) were obtained in one step from 2-hydroxybenzylamine and either *N,N*-dimethylformamide dimethyl acetal or *N,N*-dimethylacetamide dimethyl acetal under microwave irradiation (10 min., 50°C).[17] No degradation of **L2H**-**L4H** was observed in $CDCl_3$ at room temperature even after a prolonged period of time. The amphoteric character of the phenoxyamidine ligands was evidenced from **L1H**, which was converted into phenoxyamidinium bromide **[L1H$_2$][Br]** by addition of bromohydric acid or into sodium phenoxyamidine **L1Na** using NaH as a base. The proligands **L1H**-**L4H**, as well as the protonated and deprotonated form of **L1H**, were characterized by NMR spectroscopy, IR spectroscopy, exact mass and elemental analysis. The ^{1}H NMR spectrum of the phenoxyamidine proligand **L1H** (Fig. S1, SI) features a broad signal ($\Delta\nu_{1/2}$= 99.12

Hz) centered at δ = 2.85 ppm for the NMe_2 group, which is splitted into two singlets at δ = 2.91 and 3.48 ppm in the case of **[L1H$_2$][Br]** (Fig. S17, SI) attesting of the higher restricted rotation around the amidine bond when protonated. The pyrrolidine ring protons in **L2H** (Fig. S25, SI) give four poorly resolved multiplets also showing restricted rotation of the heterocycle. The NMe_2 group in **L3H** (Fig. S35) gives a slightly broadened singlet ($\Delta\nu_{1/2}$= 6.02 Hz) at δ = 2.88 ppm, while a sharp singlet at δ = 2.95 ppm ($\Delta\nu_{1/2}$= 1.26 Hz) is observed in the case of **L4H** (Fig. S40, SI).[18] Other signals in the ^{1}H NMR spectra of **L1H**-**L4H** appear well resolved with a characteristic sharp singlet integrated for two protons for the methylene linker at 4.3-4.6 ppm. The fluxional behaviors of **L1H** and **L2H** were further probed by a variable temperature ^{1}H NMR study (Fig. S7 and S31). Rotational barriers in **L1H** and **L2H** were calculated to be 55.5(10) and 61.5(5) kJ mol^{-1} from Eyring equation, significantly higher than in *N*,*N*-dimethyl-*N*'-benzylbenzamidine for which a rotational barrier of 50.2 kJ mol^{-1} has been determined.[19,20] The restricted rotation of the amidine bond is also reflected in the ^{13}C NMR spectra of **L1H** and **L2H** which display a broad signal at δ = 38.5 ppm for the NMe_2 group in **L1H** and four signals at δ = 49.3, 46.9, 25.8 and 24.9 ppm for the pyrrolidine ring in **L2H** at 298 K. Earlier studies have shown that ^{15}N chemical shifts difference ($\Delta\delta^{15}$N) between the imino and the amino nitrogen atoms of an amidine reflects the nitrogen lone pair delocalization and can be correlated with the rotational barrier for analogously substituted amidines.[21] The comparison of the $\Delta\delta^{15}$N values in **[L1H$_2$][Br]**, **L1H** and *N*,*N*-dimethyl-*N*'-benzylbenzamidine indicates a less delocalized π-system in the latter (Fig.2). The pronounced delocalization of the NR_2 lone pair in **L1H** is most probably a consequence of an intramolecular hydrogen bonding between the hydroxy group and the amidine function (see below), and may account for the restricted rotation of the amidine moiety.

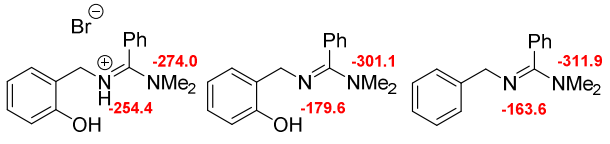

[L1H$_2$][Br] ($\Delta\delta^{15}$N = 19.6 ppm) **L1H** ($\Delta\delta^{15}$N = 121.5 ppm) ($\Delta\delta^{15}$N = 148.3 ppm)

Figure 2. ^{15}N chemical shifts (ppm) and $\Delta\delta^{15}$N values for **[L1H$_2$][Br]**, **L1H** and related *N*,*N*-dimethyl-*N*'-benzylbenzamidine.[22]

The IR spectra of **L1H**-**L4H** exhibit a very broad band between 3000 and 2100 cm^{-1} with the maximum near 2500 cm^{-1} associated with phenol with hydrogen-bonded OH stretch (Fig. S8, S33, S39 and S44). The structures of **[L1H$_2$][Br]** and **L2H** were confirmed by X-Ray diffraction analysis (Fig. 3). **[L1H$_2$][Br]** crystallizes in the *P-1* triclinic space group with two independent molecules in the asymmetric unit while **L2H** crystalizes in the *Pbca* orthorhombic space group. Both amidine and amidinium moieties adopt (*E*) configuration. In the solid state, they feature planar geometry as reflected by the sum of angles around N atoms close to 360° and torsional angles ω(N1–C1–N2–C15) close to 180°. For the two molecules, the amidine-carbon phenyl is almost orthogonal to the N–C–N "amidine plane" with a torsional angles φ(N1–C1–C9–C15) of -99.8(3)° [-104.5(3)°] in **[L1H$_2$][Br]** (the bracketed value is given for the second independent molecule present in the asymmetric unit) and 110.35(17)° in **L2H**. Concerning the phenol group, it is also orthogonal to the "amidine plane" for **[L1H$_2$][Br]**, while coplanarity is observed for **L2H** due to hydrogen bonding between the hydroxy group and the amidine function. The C–N bond lengths in **L2H** (N2–C1 1.350(2) Å; N1–C1 1.297(2) Å) range between single and double bond and are less differentiated than in analogously substituted amidine, which is consistent with a delocalized π-system.[12a] Expectedly, C–N bond lengths are almost identical in **[L1H$_2$][Br]** (N1–C1 1.323(3) Å *vs* N2–C1 1.313(3) Å [1.320(4) Å vs 1.315(3) Å]) due to a more delocalized π-system for the amidinium moiety. Noteworthy, the conformation of **L2H** observed in the solid state seems to predominate in solution at low temperature as attested by NOESY NMR experiment, which showed through-space correlations at 250 K between the phenolic proton and one pair of H_α protons of the pyrrolidine ring (Fig. S28).

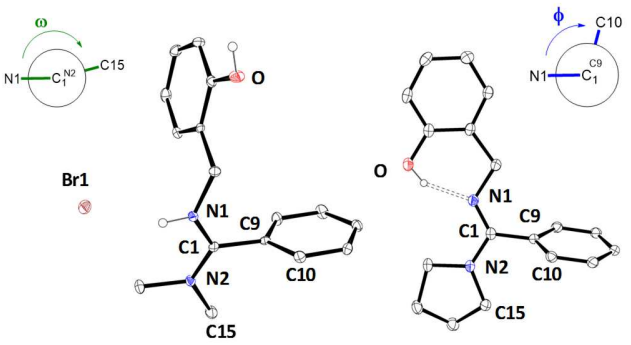

Figure 3. ORTEP views of **[L1H$_2$][Br]** (left) and **L2H** (right) and definition of torsion angles ω and φ. For [**L1H$_2$][Br]** both independent molecules exhibiting the same conformation, only one molecule is represented. Selected distances (Å) and angles (deg): **[L1H$_2$][Br]** (bracketed data correspond to the second independent molecule): C1–N1 1.323(3) [1.320(4)], C1–N2 1.313(3) [1.315(3)], ω -179.7(2) [172.9(2)], φ -99.8(3) [-104.5(3)], $\Sigma\alpha_{N2}$ 359.9(3) [359.8(4)]. **L2H**: C1–N1 1.2970(19), C1–N2 1.350(2), ω 172.11(14), φ 110.35(17), $\Sigma\alpha_{N2}$ 359.6(2).

With these proligands in our hands, their coordination chemistry with Zn(II) was first studied through reaction of equimolar amounts of **L1H**-**L4H** and Et_2Zn in hexane/THF or hexane/DCM at room temperature (Scheme 2). X-Ray analysis of single crystals of **1a** and **2a** showed that dinuclear complexes $(LZnEt)_2$ were formed in these conditions (Fig. 4). **1a** crystalizes in the *P-1* triclinic space group and two independent half-molecules are present in the asymmetric unit; the two molecules exhibiting very similar conformations. **2a** crystalizes in the *P2$_1$/c* monoclinic space group, one half molecule is present in the asymmetric unit. All Zn centers are coordinated in a pseudo tetrahedral geometry by a phenoxyamidine ligand in a *κ^{2}O,N'*-chelate fashion, one residual ethyl group and one bridging oxygen atom of the second phenoxyamidine ligand. The phenoxyamidine ligands form with the Zn(II) center 6-membered metallacycles in a boat-like conformation in the case of **1a** and half chair-like conformation for **2a**. This difference of conformation between **1a** and **2a** arises from a torsion of the phenylenemethylene linker in **2a** putting the phenylene ring into the plane defined by N, O and Zn atoms and the methylene group outward. The amidine moiety keeps the same conformation and configuration as observed in **[L1H$_2$][Br]** and **L2H**, thus with one of the alkyl substituents of the amino group on the metal side. It is worth noting that the coordination to Zn(II) has no influence on the relative C–N bond lengths of the amidine moiety: C1–N1 1.300(2) [1.308(2)] Å, 1.303(2) Å and C1–N2 1.356(2) [1.358(2)] Å, 1.343(2) Å for **1a** and **2a**, respectively. The bond lengths Zn–O and Zn–N are in the range of those observed in phenoxyimine Zn complexes.[2b] ^{1}H NMR spectra of complexes **1a**-**4a** show fluxionality in solution with a broadening of most of the signals except for the resonance associated with the phenylene linker. DOSY NMR experiments were next conducted on **1a** to determine the nuclearity of the complex in solution (Fig. S51 and tables S4-S5, SI). **1a** revealed a diffusion coefficient of 1.22 x 10^{-9} $m^2.s^{-1}$ (CD_2Cl_2, 298 K) in between the calculated value of the monomer (1,53 x 10^{-9} $m^2.s^{-1}$) and the dimer (1,13 x 10^{-9} $m^2.s^{-1}$). This average value suggests a monomer/dimer equilibrium in solution with a fast exchange at the NMR time-scale. Aiming to better understand the structure of **1a** in solution, we carried out variable-temperature ^{1}H NMR study (Fig. 5).

Scheme 2. Synthesis of the (phenoxyamidine)Zn complexes

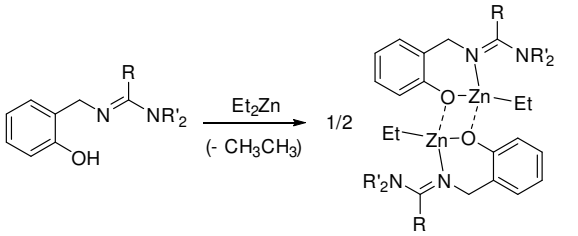

L1H-**L4H**

1a: R = Ph, R' = Me (66 %)
2a: R = Ph, R'-R'= -$(CH_2)_4$- (44 %)
3a: R = H, R' = Me (83 %)
4a: R = Me, R' = Me(86 %)

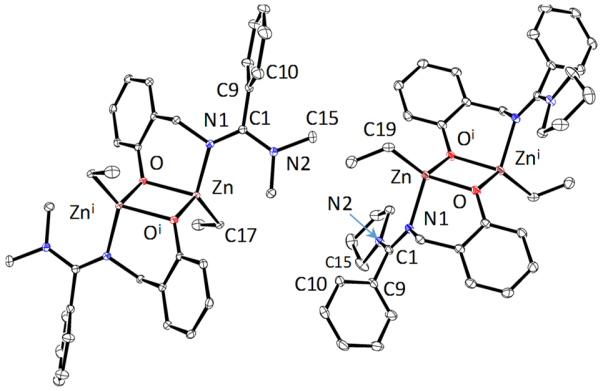

Figure 4. ORTEP views of complexes **1a** (left, only one molecule is represented) and **2a** (right) (hydrogen atoms omitted for clarity). Selected distances (Å) and angles (deg): **1a** (bracketed data correspond to the second independent molecule): Zn–O 2.0434(10) [2.0345(11)], Zn–O^{i} 2.0553(10) [2.0618(11)], Zn–N1 2.0647(13) [2.0617(13)], Zn–C17 2.0142(16) [2.0366(15)], C1–N1 1.3004(19) [1.308(2)], C1–N2 1.3562(19) [1.358(2)], O–Zn–O^{i} 83.33(4) [82.65(4)], N1–Zn–C17 131.73(6) [125.19(6)], ω 165.43(16) [-162.61(14)], φ 109.77(19) [-118.46(17)], $\Sigma\alpha_{N2}$ 360.0(2) [360.0(3)]. **2a**: Zn–O 2.0524(11), Zn–O^{i} 2.0169(11), Zn–N1 2.1069(12), Zn–C19 2.0104(16), C1–N1 1.3030(18), C1–N2 1.3426(19), O–Zn–O^{i} 82.04(4), N1–Zn–C19 107.25(6), ω 171.06(14), φ -84.7(2), $\Sigma\alpha_{N2}$ 359.8(2).

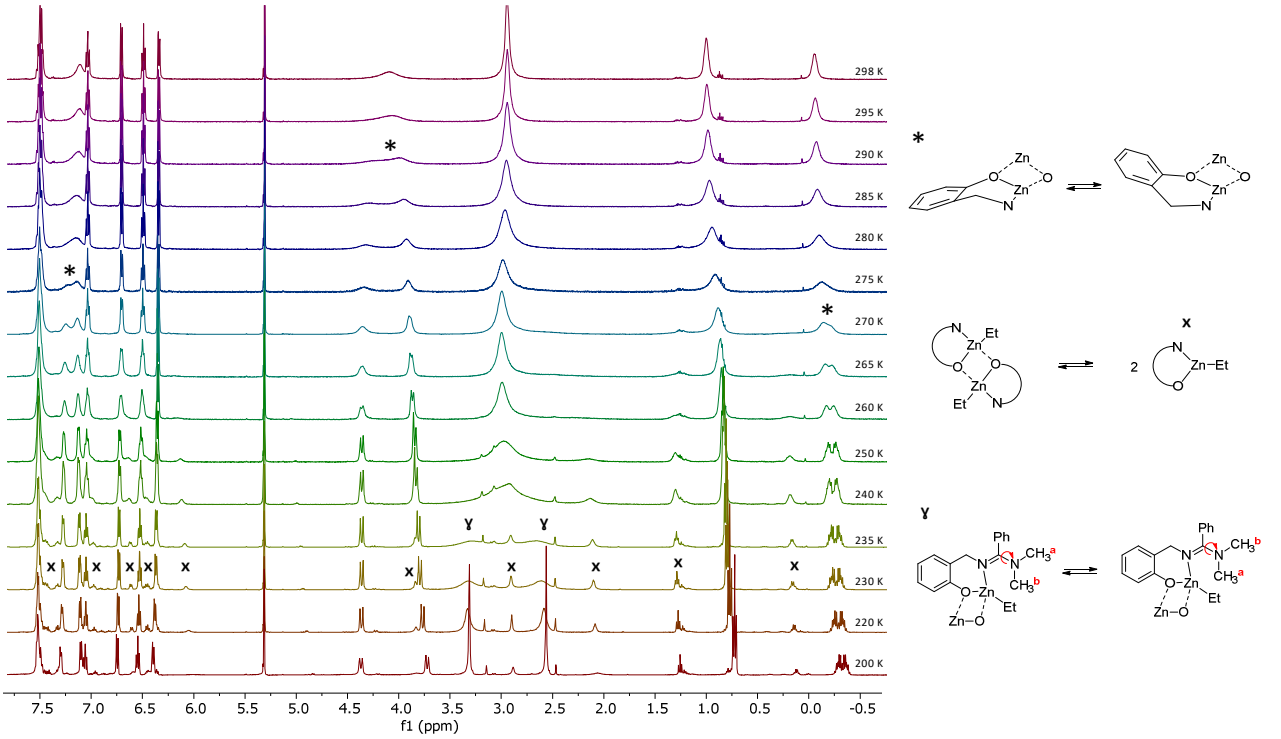

Figure 5. Variable-temperature ^{1}H NMR spectra of **1a** (600 MHz, CD_2Cl_2). Dynamic behavior of **1a** and monomer-dimer equilibrium.

Upon cooling, the benzylic CH_2 signal centered at δ = 4.13 ppm broadens and decoalesces into AB system (Tc = 292.5 K). A split of the signal of the methylene protons of the ethyl zinc ligand was observed at lower temperatures (Tc = 272.5 K). This diastereotopic splitting arises from steric constraints and restricted movement of the phenylenemethylene linkers at low temperature giving rise to sp^2-sp^3 atropoisomerism (motion and related signals labelled by "*" on Fig. 5). Additional restricted rotation of the phenyl-amidine bond gives rise to two resonances for the diastereotopic *ortho*-phenyl protons (Tc = 277.5 K). The energy barrier for the flipping motion of the 6-membered metallacycle was estimated to 55.6(5) kJ mol^{-1} from Eyring equation, which is consistent with the non-persistence of the chiral bent structure of the phenoxyamidine ethyl Zn fragment in the dinuclear complex **1a** at ambient temperature.[23] Upon further cooling (from 265 K), part of the signals decoalesces giving rise to a new set of signals that can be tentatively assigned to the monomeric complex species (signals of the monomer labelled by "x" on the spectrum registered at 230 K, Fig. 5).[24] New ethyl zinc ligand signals at δ = 0.17 and 1.31 ppm are clearly visible and correspond to a proportion of 33% of monomer at 250 K that tends to decrease at lower temperatures (21% at 200 K). With respect to the restricted rotation around the amidine bond, NMe_2 signal centered at δ = 2.95 ppm collapses below 240 K (T_C = 237.5 K) and then split into two singlets (labelled

by "γ" on Fig. 5). The corresponding smaller barrier found in **1a** (44.4(5) kJ.mol^{-1}) compared to **L1H** (55.5(5) kJ.mol^{-1}) might appear surprising at first sight, but can be rationalized considering the hydrogen bonding in the latter.

Previous studies have shown that phenoxyimine ligands have a propensity to give rather homoleptic zinc complexes (L_2Zn) than heteroleptic complexes (LZnX).[25,26] This phenomenon was not observed with **L1H**-**L4H**, so we wanted to check if bis(phenoxyamidine)Zn homoleptic complex can nevertheless be formed. To this end, we carried out the reaction between sodium phenoxyamidine salt **L1Na** and $ZnCl_2$ in 2:1 ratio and got the bis(phenoxyamidine)Zn complex **1a'** in 35 % yield after recrystallization (Scheme 3). Suitable crystals for X-Ray diffraction study were obtained by layering pentane to saturated dichloromethane solution of **1a'** (Fig. 6).

Scheme 3. Synthesis of a (phenoxyamidine)$_2$Zn complex

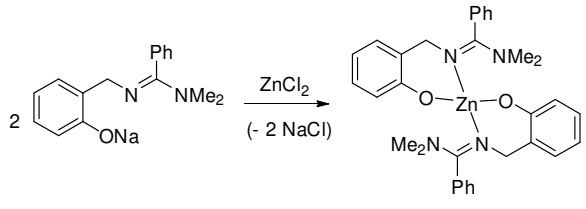

L1Na **1a'** (35 %)

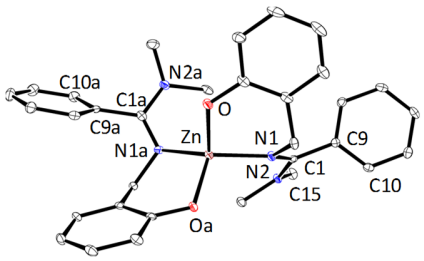

Figure 6. ORTEP view of **1a'** (hydrogen atoms are omitted for clarity). Selected distances (Å) and angles (deg), bracketed data correspond to the second ligand labeled by "a": Zn–O 1.949(2), Zn–Oa 1.940(2), Zn–N1 2.013(3), Zn–N1a 2.009(3), N1–C1 1.313(4) [1.311(4)], N2–C1 1.351(4) [1.355(4)], O–Zn–Oa 119.07(9), N1–Zn–N1a 134.46(9), ω 162.3(3) [-151.6(3)], φ 114.4(3) [-121.9(3)], $\Sigma\alpha_{N2}$ 359.6(4) [359.9(4)].

1a' crystallizes in the *P2$_1$/c* monoclinic space group. Zn atom links two phenoxyamidine ligands in a pseudo tetrahedral geometry giving rise to a chiral spiro-complex with an approximate C2 symmetry. Both metallacycles adopt a half chair-like conformation similar to the one observed for complex **2a**. The chirality of the complex **1a'** is reflected in the ^{1}H NMR spectrum by a diasterotopic splitting of the benzylic CH_2 protons signals into a set of two doublets (AB spin system, Fig. S68). Diastereotopicity is also observed for the *ortho*-protons of the phenyl ring, due to the restricted rotation of the phenyl-amidine bond.

Phenoxyamidine ligands were coordinated to Al(III) *via* an alkane elimination route similar to the one used in Zn series. Thus, the phenol-amidine proligands **L1H**-**L4H** were reacted with $AlMe_3$ in THF or DCM at room temperature to yield the phenoxyamidine dimethyl aluminium complexes **1b**-**4b** in 75 to 85% yields (Scheme 4). Compared with Zn(II) analogues, the ^{1}H NMR spectra of Al(III) complexes show sharper signals along with a more upfield shielded signal of the methylene linker (Δδ = 0.2 ppm). A single ^{1}H NMR signal from NMe_2 group in complexes **1b**, **3b** and **4b** and only two signals for the pyrrolidine ring in **2b** are displayed on spectra, which is consistent with a fast rotation around the amidine bond with respect to NMR time scale at room temperature (Fig. S73, S79, S85, S90). Consistently, phenyl-amidine bond rotational barrier of 51.9(5) kJ mol^{-1} was determined in complex **2b** by VT NMR study (Fig. S83).[19] X-Ray diffraction study of complexes **1b** (monoclinic, *P2$_1$/c*) and **2b** (monoclinic, *P2$_1$/n*) revealed a pseudo-tetrahedral geometry around the Al atom, which forms with the phenoxyamidine ligand a 6-membered metallacycle in a boat like conformation (Fig. 7).

Scheme 4. Synthesis of the (phenoxyamidine)Al complexes

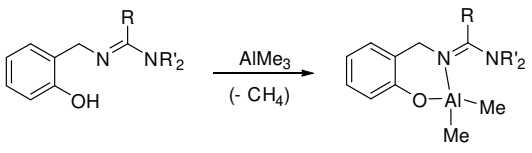

L1H-**L4H**

1b: R = Ph, R' = Me (77 %)
2b: R = Ph, R'-R'= -(CH$_2$)$_4$- (75 %)
3b: R = H, R' = Me (76 %)
4b: R = Me, R' = Me (85 %)

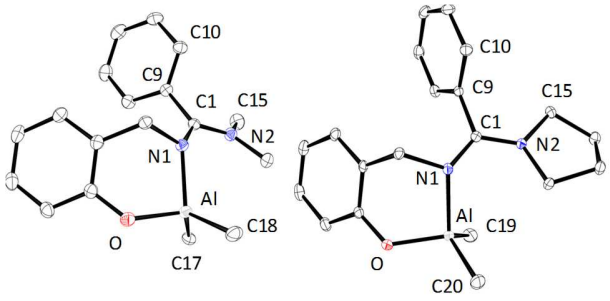

Figure 7. ORTEP views of **1b** (left) and **2b** (right) (hydrogen atoms omitted for clarity). Selected distances (Å) and angles (deg): **1b**: Al–O 1.7769(13), Al–N1 1.9601(14), Al–C17 2.0051(19), Al–C18 1.9757(19), N1–C1 1.324(2), N2–C1 1.337(2), O–Al–N1 96.58(6), C17–Al–C18 117.74(8), ω 163.83(15), φ 112.22(18), $\Sigma\alpha_{N2}$ 360.0(2). **2b**: Al–O 1.7874(13), Al–N1 1.9674(15), Al–C19 1.9690(19), Al–C20 1.962(2), N1–C1 1.314(2), N2–C1 1.334(2), O–Al–N1 97.06(6), C19–Al–C20 119.06(9), ω 170.82(15), φ 106.77(19), $\Sigma\alpha_{N2}$ 359.9(2).

The geometry of the amidine fragment is similar to the one observed in Zn complexes **1a** and **2a** but with smaller difference between C=N and C–N bond lengths (Δ_{CN} = 0.013(3) Å and 0.019(3) Å in **1b** and **2b**, respectively). Analogous phenoxyimine dimethyl aluminum complex reported by Nomura shows similar tetrahedral geometry around Al, a nearly planar 6-membered metallacycle, shorter Al–C bond lengths and a longer Al–N bond length probably due to the less electron donating ability of imines with respect to amidines.[2c]

ROP of Lactide. The heteroleptic Zn(II) and Al(III) complexes **1a-4a** and **1b-4b**, respectively, were tested as ROP initiators for *rac*-lactide ROP in the presence of 1 equiv. of ^{i}PrOH or BnOH as the alcohol source. The results are compiled in Table 1. All Zn(II) species readily polymerize lactide (100 equiv) at room temperature within 2 to 7 h to afford atactic PLA, as deduced from NMR and SEC data (Fig. S101-106). The phenoxyamidine Zn complexes **1a-4a** give rise to apparent TOF up to 50 mol of LA (mol of Zn)$^{-1}$ h^{-1}. These values are higher than that of the phenoxyimine chelate Zn complexes reported by Chisholm[26] (apparent TOF up to 6 mol of LA (mol of Zn)$^{-1}$ h^{-1}) but do not compare with the most active Zn catalysts reported to date.[27]

Table 1. ROP of lactide mediated by **1a**-**4a** and **1b**-**4b**[a]

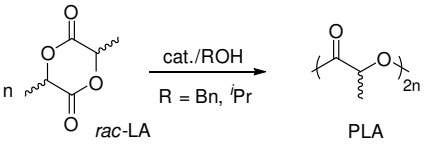

Run	Cat.	ROH	Time (h)[b]	T (°C)	Conv (%)[c]	$M_{n,exp}$[e] ($M_{n,theo}$[d])	Đ[f]
1	**1a**[g]	^{i}PrOH	2	RT	99	9300 (14200)	1.53
2	**2a**[g]	^{i}PrOH	2	RT	96	14700 (13800)	1.02
3	**2a**[g]	BnOH[i]	7[i]	RT	100	12700 (14300)	1.08
4	**3a**[g]	^{i}PrOH	2	RT	96	15250 (13800)	1.83
5	**4a**[g]	^{i}PrOH	2	RT	98	12900 (14100)	1.65
6	**1b**[h]	^{i}PrOH	24	70	94	4700 (13550)	1.29
7	**2b**[h]	^{i}PrOH	24	70	56	7400 (8100)	1.06
8	**2b**[h]	^{i}PrOH	12	90	97	12900 (14000)	1.05
9	**2b**[h]	BnOH	10	90	100	12100 (14400)	1.07

10	**3b**[h]	^{i}PrOH	24	70	89	3500 (12830)	2.17
11	**4b**[h]	^{i}PrOH	24	70	98	6900 (14100)	1.40

[a]Polymerization conditions: [*rac*-LA]$_0$ = 1 M, 100 equiv of *rac*-LA, 1 equiv of ROH (^{i}PrOH or BnOH) and 1 equiv of metal catalyst. [b]Reaction time. [c]Monomer conversion. [d] Calculated using $M_{n,theo}$ = [*rac*-LA]$_0$/[catalyst]$_0$ × M_{LA} × conversion. [e]Measured by GPC in THF (30 ˚C) using PS standards and corrected by applying the appropriate correcting factor (0.58). [f] Measured by GPC in THF (30 ˚C). [g] in CH_2Cl_2, room temperature. [h] in toluene. [i] not optimized.

A comparison between **1a**, **3a** and **4a** shows that modification of the ligand backbone has little influence on activity. These results contrast with those of Lin and co-workers, who has shown that tridentate Schiff base Zn complexes bearing Ph or Me substituent on the imine-carbon showed much higher catalytic activities than salicylaldimine derivatives.[2b,28] For all Zn(II) species (**1a**-**4a**), the formed PLA is chain-length controlled in good agreement with the expected values, though narrow disperse PLA ($Đ$ < 1.1) is only produced with catalyst **2a**, which incorporates a phenyl group on the amidine carbon and a more sterically hindered pyrrolidine-amidine moiety (entries 2 and 3, Table 1). Kinetic data gathered for catalysts **1a** and **2a** agree with a controlled ROP in both cases, including: i) a linear correlation between the PLA Mn values and lactide conversion as the ROP proceeds (Fig. S98 and S100); ii) a reaction rate law observed to be first order in monomer (Fig. S99).

^{1}H NMR monitoring experiments of a 1/1 **1a**/^{i}PrOH mixture in CD_2Cl_2 showed ethane evolution and the formation of an alkoxy complex **1a"** along with other species that were identified as the homoleptic complex **1a'** and EtZn(O^{i}Pr) (Fig. S95-S96). Both Zn–OR species **1a''** and EtZn(O^{i}Pr) may account for the observed lactide ROP activity of the **1a**/^{i}PrOH catalytic system. X-Ray diffraction study conducted on a single crystal of **1a"** (triclinic, *P-1*) grown from the NMR sample confirmed the formation of an alkoxy complex revealing a dinuclear Zn complex bridged by the oxygen atom of the isopropoxy groups (Fig. 8). The geometry around the Zn atoms is pseudo tetrahedral. Both (phenoxyamidine)Zn metallacycles feature boat like conformation folded in the same direction. The amidine moiety in **1a"** is in *E*-configuration with planar arrangement and with slightly smaller difference between the C=N and C–N bond lengths (Δ_{CN} = 0.036(3) and 0.030(3) Å) than in **1a** (Δ_{CN} = 0.056(3) Å). In the case of **2a**/BnOH, MALDI-TOF data of the produced PLA are consistent with a BnO-end-capped linear PLA. The latter is in line with a ROP process occurring through a coordination-insertion mechanism from an *in situ* formed Zn-OBn species that acts as the actual catalyst.

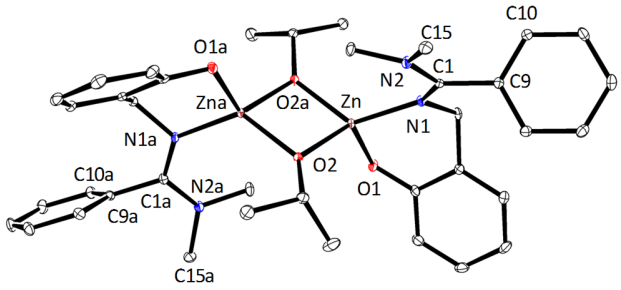

Figure 8. ORTEP view of **1a"** (hydrogen atoms are omitted for clarity). Selected distances (Å) and angles (deg), bracketed data correspond to the second moiety labeled by "a": Zn–O2 1.9548(11), Zn–O2a 1.9561(13), Zn–O1 1.9276(12) [1.9252(12)], Zn–N1 2.0090(14) [2.0043(13)], Zna–O2 1.9514(12), Zna–O2a 1.9639(12), N1–C1 1.310(2) [1.314(2)], N2–C1 1.345(2) [1.343(2)], O2a–Zn–O2 82.86(5), O2a–Zna–O2 82.75(5), O1–Zn–N1 99.24(5) [99.21(6)], ω 170.67(16) [163.74(16)], φ 105.64(19) [110.91(19)], $\Sigma\alpha_{N2}$ 360.0(3) [360.0(3)].

When using catalyst **4a**, the ROP of lactide proceeds with a moderate control leading to the production of broadly disperse PLA, which is likely due to the formation of linear and cyclic PLA as deduced from MALDI-TOF data (Fig. S105-S106). As summarized in Table 1, Al(III) complexes **1b**-**4b** all mediate the ROP of lactide (70 °C or 90 °C, toluene) in the presence of ^{i}PrOH/BnOH, albeit with a moderate activity (apparent TOF up to 10 mol of LA (mol of Al)$^{-1}$ h^{-1}) comparable to those reported by Carpentier,[29] Nomura,[30] Chen,[6] Redshaw[31] and Pappalardo[2d] with Al(III) Schiff base initiators.[32] Similarly to the Zn(II)

analogues, the pyrrolidine-incorporating derivative **2b** performs best whether regarding ROP control and activity to afford narrow disperse and chain-length controlled PLA in good agreement with the expected PLA M_ns (entries 7-9, Table 1). In contrast, PLAs with a broader polydispersity (ranging from 1.29 to 2.17) and lower M_n values than theoretically expected are produced using less sterically hindered catalysts **1b**, **3b** and **4b** in combination with ^{i}PrOH (entries 6, 10 and 11, Table 1), indicating a poorly controlled ROP process. The latter likely indicates an ill-defined ROP catalytic system, presumably due to the sluggish activation of Al dialkyl precursors **1b**, **3b** and **4b** by ^{i}PrOH, as suggested by ^{1}H NMR monitoring experiments. Kinetic data for lactide ROP initiated by **2b**/BnOH all support a well-controlled ROP process (Fig. S108-S112) and MALDI-TOF data are consistent with a BnO-ended linear PLA (S113 and S114). Overall, within the ligand series, the better ROP performances of the pyrrolidine-bearing metal complexes (**2a** and **2b**) clearly indicate that substantial steric protection of the Zn(II)/Al(III) metal centers is beneficial to lactide ROP control and the production of narrow disperse PLA.

Conclusion

We have developed the synthesis of new ditopic ligands, which combine a phenoxy group and a *N*,*N*,*N*'-trisubstituted amidine spaced by a methylene linker. The coordination chemistry of these ligands has been investigated with Zn(II) and Al(III) metal ions resulting in a variety of discrete metal complexes. Phenoxyamidines behave as bidentate ligands coordinated through O and N' donor atoms. In the solid state, phenoxyamidines feature planar geometry and *E*-configuration with little difference between C=N and C–N bond lengths highlighting the conjugated character of the amidine function. In the Zn(II) and Al(III) complexes, the amino NR'$_2$ group of the amidine function does not bind to the metal but provides steric bulk about it. NMR studies have shown that the phenoxyamidine complexes are fluxional in solution with both a flipping motion of the metallacycle and the rotation about the C–N amidine bond. With respect to lactide polymerization activity, the heteroleptic phenoxyamidine Zn(II)–/Al(III)–alkyl complexes in combination with an alcohol source were found all active in lactide ROP catalysis and afforded atactic PLA. A superior ROP control was achieved with the more sterically protected Zn(II) and Al(III) complexes **2a** and **2b**.

EXPERIMENTAL SECTION

General consideration. All reactions, except when indicated, were carried out under an atmosphere of argon using conventional Schlenk techniques and Ar glovebox. DCM, diethyl ether, THF, toluene, and pentane were dried using a MBRAUN SPS 800. Microwave experiments were performed on a monowave 300 Anton-Paar apparatus (monomode microwave) with infrared detection of temperature. Analyses were performed at the "Plateforme d'Analyses Chimiques de Synthèse Moléculaire de l'Université de Bourgogne" and for some elemental analyses also at the London Metropolitan University, especially for sensitive compounds. The identity and purity of the compounds were established using elemental analyses, multinuclear NMR spectroscopy, X-ray diffraction analysis, and high-resolution mass spectrometry. NMR spectra (^{1}H, ^{13}C, ^{15}N) were recorded on Bruker 300 Avance III, Bruker 500 Avance III, or Bruker 600 Avance III spectrometers. All acquisitions were performed at 300 K. Chemical shifts are quoted in parts per million (δ) relative to TMS (for ^{1}H and ^{13}C). For ^{1}H and ^{13}C spectra, values were determined by using solvent residual signals (*e.g.* $CHCl_3$ in $CDCl_3$) as internal standards. Assignment of ^{1}H and ^{13}C signals (when possible) was done through the use of 2D experiences (COSY, HSQC and HMBC). High resolution mass spectra were recorded on a Thermo LTQ Orbitrap XL ESI-MS (ElectroSpray Ionization Mass Spectrometry). Chlorobenziminium chloride derivatives were synthesized according to previously reported procedure.[33] All other reagents were commercially available and used as received.

X-Ray experimental procedure. Crystal of all compound were selected and mounted on a mylar loop with oil on either a 'Bruker APEX-II CCD' or a 'Bruker D8 venture Photon 100' diffractometer. Crystal were kept at 115 K or 100 K during data collection. Using Olex2,[34] the structures were solved with the ShelXT[35] structure solution program using Direct Methods and refined with the XL[36] refinement package using Least Squares minimization. More details can be found in the Supporting Information

and in the Crystallographic Information Files in which are imbedded the .res and .hkl files.

Synthesis of (*E*)-*N'*-(2-hydroxybenzyl)-*N*,*N*-dimethylbenzamidine L1H (light yellow solid, 1.9 g, yield: 76 %). *N*,*N*-dimethylchlorobenziminium chloride (1 equiv., 10 mmol, 2.12 g) was solubilized in DCM (30 mL) and cooled to 0 °C. Triethylamine (5 equiv., 50.0 mmol, 6.95 mL) was added, and then slowly 50 mL of DCM solution of 2-hydroxybenzylamine (1 equiv., 10 mmol, 1.23 g). The mixture was stirred at 0°C for 15' and then at r.t. for 1h30. After hydrolysis and extraction with DCM, the combined organic layer was dried (anhydrous $MgSO_4$), filtered, and concentrated in vacuo. The residue was washed successively with ether and pentane to give **L1H**. **HRMS (ESI-pos):** calcd for $[C_{16}H_{19}N_2O]^+$ [M + H]$^+$: 255.14919. Found: 255.14804 (-4.5 ppm). **Elemental Analysis:** calcd for $C_{16}H_{18}N_2O$: C, 75.56; H, 7.13; N, 11.01 %. Found: C, 75.22; H, 7.51; N, 10.78 %. **^{1}H NMR** (600 MHz, CD_2Cl_2): δ (ppm) = 7.51-7.45 (m, 3H, *m*-Ph and *p*-Ph), 7.18-7.16 (m, 2H, *o*-Ph), 7.04 (m, 1H, Ar H_4), 6.74 (d, $^3J_{H\text{-}H}$ = 8.2 Hz, 1H, Ar H_3), 6.66-6.62 (m, 2H, Ar H_5 and Ar H_6), 4.23 (s, 2H, $ArCH_2$), 2.85 (broad s, 6H, NMe_2). **^{13}C{^{1}H} NMR** (151 MHz, CD_2Cl_2), δ (ppm): 163.1 (C_q, C=N), 158.9 (C_q, C–O), 133.6 (C_q, *i*-Ph), 129.4 (CH, *p*-Ph), 129.4 (CH, *m*-Ph), 127.8 (CH, *o*-Ph overlapping with Ar C_4), 127.5 (CH, Ar C_6), 125.6 (C_q, Ar C_1), 118.7 (CH, Ar C_5), 116.7 (CH, Ar C_3), 55.0 (CH_2, Ar*C*H_2), 38.5 (bs, CH_3, NMe_2). **^{1}H ^{15}N HMBC** (600.23 MHz / 43.3 MHz, CD_2Cl_2,): δ ^{1}H / δ ^{15}N (ppm) = 4.23 / -179.6 ($ArCH_2$ / N imino), 4.23 / -301.1 ($ArCH_2$ / N amino).

Synthesis of (*E*)-*N'*-(2-hydroxybenzyl)-*N*,*N*-dimethylbenzamidinium bromide [L1H$_2$][Br] (white solid, 52 mg, 79 %). 50 µl of hydrobromic acid (48 wt. % in H_2O) were added to DCM solution (3 mL) of **L1H** (50 mg, 0.2 mmol) cooled to 0 °C in an ice bath. The mixture was stirred for 30 minutes at room temperature, during which time a white precipitate was formed. The supernatant was removed by filtration and the residue was dried under vacuum to give the amidinium salt **[L1H$_2$][Br]**. **HRMS (ESI-pos):** calcd for $[C_{16}H_{19}N_2O - Br]^+$ [M]$^+$: 255.14919. Found: 255.14947 (1.1 ppm). **Elemental Analysis:** calcd for $C_{16}H_{19}BrN_2O$: C, 57.32; H, 5.71; N, 8.36 %. Found: C, 57.51; H, 5.52; N, 7.99 %. **^{1}H NMR** (500 MHz, $CDCl_3$): δ (ppm) = 9.50 (broad, 1H, NH), 8.53 (broad, 1H, OH), 7.58 (m, 1H, *p*-Ph), 7.50 (m, 2H, *m*-Ph), 7.24 (m, 2H, *o*-Ph), 7.16 (dd, $^3J_{HH}$ = 8.1 Hz, $^4J_{HH}$ = 1.2 Hz, 1H, Ar H_3), 7.04 (pseudo td, $^3J_{HH}$ = 7.8 Hz, $^4J_{HH}$ = 1.7 Hz, 1H, Ar H_4), 6.58 (pseudo td, $^3J_{HH}$ = 7.4 Hz, $^4J_{HH}$ = 1.2 Hz, 1H, Ar H_5), 6.42 (d, $^3J_{HH}$ = 7.4 Hz, 1H, Ar H_6), 4.32 (d, $^3J_{HH}$ = 4.8 Hz, 2H, $ArCH_2$), 3.48 (s, 3H, NMe), 2.91 (s, 3H, NMe). **^{13}C{^{1}H} NMR** (126 MHz, $CDCl_3$): δ (ppm) = 165.1 (C_q, C=N), 155.3 (C_q, C–O), 132.2 (CH, *p*-Ph), 129.9 (CH, *m*-Ph), 129.7 (CH, Ar C_4), 129.4 (CH, Ar C_6) 127.7 (CH, *o*-Ph), 127.0 (C_q, *i*-Ph), 122.5 (C_q, Ar C_1), 119.7 (CH, Ar C_5), 117.6 (CH, Ar C_3), 46.5 (CH_2, Ar*C*H_2), 42.6 (CH_3, NMe), 41.0 (CH_3, NMe). **^{1}H ^{15}N HMBC** (600.23 MHz / 43.3 MHz, CD_2Cl_2): δ ^{1}H / δ ^{15}N (ppm) = 4.32 / -254.4 ($ArCH_2$ / N imino), 3.48 / -254.4 (NMe / N imino), 3.48 / -274.0 (NMe / N amino), 2.91 / -274.0 (NMe / N amino).

Synthesis of L1Na (white solid, 0.83 g, yield: 70 %). *N'*-(2-hydroxybenzyl)-*N*,*N*-dimethylbenzamidine **L1H** (1 equiv., 4.3 mmol, 1.1 g) and NaH (2 equiv., 95 % purity, 8.6 mmol, 208 mg) were suspended in THF (20 mL) and stirred 2 h. Stirring was stopped and a resulting white salt was let to settle. The supernatant was cannulated with a borosilicate filter. The filtrate was concentrated to give a white solid which was washed with DCM (2 x 10 mL) to give the product as a white solid. **Elemental Analysis:** calcd for $C_{16}H_{17}N_2NaO$: C, 69.55; H, 6.20; N, 10.14 %. Found: C, 68.48; H, 6.32; N, 10.24 %. **^{1}H NMR** (500 MHz, THF-d_8): δ (ppm) = 7.44 (m, 2H, *m*-Ph), 7.41 (m, 1H, *p*-Ph overlapping with *m*-Ph), 7.04 (m, 2H, *o*-Ph), 6.75 (pseudo td, $^3J_{HH}$ = 7.6 Hz, $^4J_{HH}$ = 2.0 Hz, 1H, Ar H_4), 6.44 (d, $^3J_{HH}$ = 8.0 Hz, 1H, Ar H_3), 6.21 (dd, $^3J_{HH}$ = 7.2 Hz, $^4J_{HH}$ = 2.0 Hz, 1H, Ar H_6), 5.97 (pseudo t, $^3J_{HH}$ = 7.1 Hz, 1H, Ar H_5), 4.13 (s, 2H, $ArCH_2$), 2.46 (s, 6H, NMe_2). **^{13}C{^{1}H} NMR** (126 MHz, THF-d_8): δ (ppm) = 170.7 (C_q, C–O), 163.4 (C_q, C=N), 136.5 (C_q, *i*-Ph), 130.6 (C_q, Ar C_1), 130.4 (CH, Ar C_6), 129.2 (CH, *o*-Ph), 129.1 (CH, *m*-Ph), 129.0 (CH, *p*-Ph), 128.5 (CH, Ar C_4), 119.8 (CH, Ar C_3), 110.7 (CH, Ar C_5), 54.7 (CH_2, Ar*C*H_2), 38.4 (CH_3, NMe_2).

Synthesis of (*E*)-*N'*-(2-hydroxybenzyl)pyrrolidinylbenzamidine L2H (white powder, 2.45 g, yield: 87 %). Same procedure than for **L1H** using pyrrolidinylchlorobenziminium chloride instead of *N*,*N*-dimethylchlorobenziminium chloride. **HRMS (ESI-pos):** calcd for $[C_{18}H_{21}N_2O]^+$ [M + H]$^+$: 281.16484. Found: 281.16277 (-1.9 ppm). **Elemental Analysis:** calcd for $C_{18}H_{20}N_2O$: C, 77.11; H, 7.19; N, 9.99 %. Found: C, 76.94; H, 7.41; N, 9.88 %. **^{1}H NMR** (500

MHz, $CDCl_3$), δ (ppm): 11.81 (broad, 1H, OH), 7.50-7.46 (m, 3H, *m*-Ph and *p*-Ph), 7.19 (m, 2H, *o*-Ph), 7.07 (m, 1H, Ar H_4), 6.85 (d, $^3J_{H\text{-}H}$ = 8.0 Hz, 1H, Ar H_3), 6.67-6.61 (m, 2H, Ar H_5 and Ar H_6), 4.33 (s, 2H, $ArCH_2$), 3.62 (broad, 2H, NCH_2CH_2), 3.03 (broad, 2H, NCH_2CH_2), 1.97 (broad, 2H, NCH_2CH_2), 1.82 (broad, 2H, NCH_2CH_2). **$^{13}C\{^1H\}$ NMR** (126 MHz $CDCl_3$), δ (ppm): 160.3 (C_q, C=N), 158.5 (C_q, C–O), 133.7 (C_q, *i*-Ph), 129.4 (CH, *p*-Ph), 129.2 (CH, *m*-Ph), 127.8 (CH, Ar C_4), 127.4 (CH, Ar C_6), 127.2 (CH, *o*-Ph), 125.1 (C_q, Ar C_1), 118.6 (CH, Ar C_5), 117.0 (CH, Ar C_3), 53.8 (CH_2, $ArCH_2$), 49.3 (CH_2, NCH_2CH_2), 46.9 (CH_2, NCH_2CH_2), 25.8 (CH_2, NCH_2CH_2), 24.9 (CH_2, NCH_2CH_2). **^1H ^{15}N HMBC** (600.23 MHz / 43.3 MHz, $CDCl_3$, 250 K): δ ^1H / δ ^{15}N (ppm) = 4.33 / -194.4 ($ArCH_2$ / N imino), 1.96 / -274.1 (NCH_2CH_2 / N amino), 1.79 / -274.1 (NCH_2CH_2 / N amino).

Synthesis of (*E*)-*N'*-(2-hydroxybenzyl)-*N*,*N*-dimethylformamidine L3H (pale yellow solid, 0.642 g, yield: 90 %). *N,N*-Dimethylformamide dimethylacetal (1 equiv., 97 % purity, 4.00 mmol, 0.491 g) in DCM (8 mL) was added to 2-hydroxybenzylamine (1 equiv., 4.00 mmol, 0.493 mg) in a microwave vial. The yellow solution was stirred 10 min under MW irradiation at 50 °C. Volatiles were evaporated then DCM/pentane mixture (25 mL) was added. The brown solid was filtered and the solvent evaporated to afford the product **L3H**. **HRMS (ESI-pos):** calcd for $[C_{10}H_{15}N_2O]^+$ $[M + H]^+$: 179.11789. Found: 179.11699 (-5.0 ppm). **Elemental Analysis:** calcd for $C_{10}H_{14}N_2O$: C, 67.39; H, 7.92; N, 15.72 %. Found: C, 67.55; H, 7.80; N, 15.55 %. **^1H NMR** (600 MHz, $CDCl_3$): δ (ppm) = 9.89 (broad, 1H, OH), 7.34 (s, 1H, CH formamidine), 7.11 (pseudo td, $^3J_{HH}$ = 7.8 Hz, $^4J_{HH}$ = 1.7 Hz, 1H, Ar H_4), 6.95 (dd, $^3J_{HH}$ = 7.5 Hz, $^4J_{HH}$ 1.6 Hz, 1H, Ar H_6), 6.84 (dd, $^3J_{HH}$ = 8.1 Hz, $^4J_{HH}$ = 1.2 Hz, 1H, Ar H_3), 6.76 (pseudo td, $^3J_{HH}$ = 7.4, $^4J_{HH}$ = 1.2 Hz, 1H, Ar H_5), 4.59 (s, 2H, CH_2), 2.88 (s, 6H, NMe_2). **$^{13}C\{^1H\}$ NMR** ($CDCl_3$, 151 MHz), δ (ppm): 157.7 (Cq, Ar C–O), 154.6 (Cq, C=N), 127.9 (CH, Ar C_4), 127.0 (CH, Ar C_3), 125.6 (Cq, Ar C_1), 118.9 (CH, Ar C_5), 116.8 (CH, Ar C_6), 58.7 (CH_2, $ArCH_2$), 40.1 (broad, CH_3, NMe_2), 34.7 (broad, CH_3, NMe_2). **HMBC** (600.23 MHz / 43.3 MHz, $CDCl_3$): δ ^1H / δ ^{15}N (ppm) = 7.32 / -185.3 (*H*C=N / N imino), 7.32 / -307.7 (*H*C=N / N amino), 4.59 / -185.3 ($ArCH_2$ / N imino), 2.88 / -307.7 (NCH_3 / N imino).

Synthesis of (*E*)-*N'*-(2-hydroxybenzyl)-*N*,*N*-dimethylacetamidine L4H (pale yellow solid, 0.650 g, yield: 85 %). Same procedure than for **L3H** using *N,N*-Dimethylacetamide dimethylacetal instead of *N,N*-Dimethylformamide dimethylacetal. **HR-MS (ESI-pos):** calcd for $[C_{11}H_{17}N_2O]^+$ $[M + H]^+$: 193.13354. Found: 193.13303 (-2.6 ppm). **Elemental Analysis:** calcd for $C_{11}H_{16}N_2O$: C, 68.72; H, 8.39; N, 14.57 %. Found: C, 68.56; H, 8.79; N, 14.53 %. **^1H NMR** (500 MHz, CD_2Cl_2): δ (ppm) = 11.47 (broad, 1H, OH), 7.05 (m, 1H, H_4), 6.96 (m, 1H, H_3), 6.73-6.69 (m, 2H, H_5 and H_6), 4.58 (s, 2H, CH_2), 2.95 (s, 6H, NMe_2), 2.00 (s, 3H, CH_3 acetamidine). **$^{13}C\{^1H\}$ NMR** (151 MHz, CD_2Cl_2), δ (ppm): 160.0 (Cq, Ar C–O), 158.9 (Cq, C=N), 127.3 (CH, Ar C_3 overlapping with ArC_4), 124.3 (Cq, Ar C_1), 118.1 (CH, Ar $C_{5/6}$), 116.5 (CH, Ar $C_{5/6}$), 53.6 (CH_2, $ArCH_2$), 38.2 (CH_3, NMe_2), 12.6 (CH_3, acetamidine). **HMBC** (600.23 MHz / 43.3 MHz, $CDCl_3$): δ ^1H / δ ^{15}N (ppm) = 4.58 / -183.1 ($ArCH_2$ / N imino), 2.95 / -299.4 (NMe / N amino), 1.99 / -183.1 (acetamidine / N imino), 1.99 / -299.4 (acetamidine / N amino).

Synthesis of 1a (orange crystals, 230 mg, yield: 66 %). THF solution (20 mL) of **L1H** (1 equiv., 1.00 mmol, 254 mg) was slowly added to a Schlenk flask containing a diethylzinc solution (1 equiv., 1 M in hexanes, 1.00 mmol, 1.00 mL). The mixture was stirred for 2 h at rt. The volatiles were evaporated. The residual solid was recrystallized by layering technique using a DCM/pentane system. After several days, the complex **1a** was obtained as orange crystals (230 mg, 66 %). **Elemental Analysis:** calcd for $C_{36}H_{44}N_4O_2Zn_2$: C, 62.17; H, 6.38; N, 8.06 %. Found: C, 61.95; H, 6.46; N, 7.97 %. **^1H NMR** (500 MHz, THF-d_8): δ (ppm) = 7.51 (broad, 4H, *m*-Ph), 7.49 (broad, 2H, *p*-Ph overlapping with *m*-Ph), 7.13 (broad, 4H, *o*-Ph), 6.95 (pseudo t, $^3J_{HH}$ = 7.7 Hz, 2H, Ar H_4), 6.69 (d, $^3J_{HH}$ = 8.0 Hz, 2H, Ar H_3), 6.40 (pseudo t, $^3J_{HH}$ = 7.3 Hz, 2H, Ar H_5), 6.28 (d, $^3J_{HH}$ = 7.3 Hz, 2H, Ar H_6), 4.13 (broad, 4H, $ArCH_2$), 2.95 (broad, 12H, NMe_2), 1.04 (t, $^3J_{HH}$ = 8.1 Hz, 6H, CH_2CH_3), 0.01 (q, $^3J_{HH}$ = 8.1 Hz, 4H, CH_2CH_3). **$^{13}C\{^1H\}$ NMR** (THF-d_8, 126 MHz,): δ (ppm) = 168.9 (C_q, C=N), 164.5 (C_q, C–O), 134.5 (C_q, *i*-Ph), 130.5 (CH, *p*-Ph), 130.1 (C_q, Ar C_1), 129.5 (2 overlapping CH, *m*-Ph and Ar C_6), 129.3 (CH, *o*-Ph), 129.0 (CH, Ar C_4), 120.2 (CH, Ar C_3), 116.4 (CH, Ar C_5), 55.0 (CH_2, $ArCH_2$), 40.2 (CH_3, NMe_2), 13.3 (CH_3, ZnEt), 0.5 (CH_2, ZnEt).

Synthesis of 2a (white crystals, 108 mg, yield: 44 %). Diethylzinc solution (1M in hexanes, 0.655 mL, 0.656 mmol, 1equiv.) was slowly added into DCM solution of **L2H** (183.8 mg, 0.656 mmol, 1equiv.). The mixture was

stirred 2 h at room temperature. The volatiles were evaporated and the residual solid was purified by recrystallization using a DCM/diethyl ether biphasic system. **Elemental analysis:** calcd for $C_{40}H_{48}N_4O_2Zn_2$: C, 64.25; H, 6.47; N, 7.49 %. Found: C, 62.45; H, 6.84; N, 7.54 %. **^{1}H NMR** (500 MHz, CD_2Cl_2), δ (ppm): 7.50 (broad, 6H, Ph), 7.09 (broad, 4H, Ph), 7.04 (pseudo t, $^3J_{H\text{-}H}$ = 7.8 Hz, 2H, Ar H_4 overlapping Ph), 6.67 (d, $^3J_{H\text{-}H}$ = 7.9 Hz, 2H, Ar H_3), 6.47 (pseudo t, $^3J_{H\text{-}H}$ = 7.3 Hz, 2H, Ar H_5), 6.30 (d, $^3J_{H\text{-}H}$ = 7.3 Hz, 2H, Ar H_6), 4.12 (broad, 4H, $ArCH_2$), 3.35 (broad, 8H, NCH_2CH_2), 1.80 (broad, 8H, NCH_2CH_2), 1.07 (broad, 6H, CH_2CH_3), 0.00 (broad, 4H, CH_2CH_3). **^{13}C{^{1}H} NMR** (126 MHz, CD_2Cl_2), δ (ppm): 164.9 (C_q, C=N), 164.1 (C_q, C–O), 135.1 (C_q, *i*-Ph), 129.8 (C_q, Ar C_1), 129.7 (CH, Ar C_6), 129.3 (2 overlapping CH, Ph), 128.8 (CH, Ar C_4), 127.9 (CH, Ph), 119.9 (CH, Ar C_3), 116.1 (CH, Ar C_5), 53.9 (CH_2, $ArCH_2$), 49.8 (CH_2, NCH_2CH_2), 25.6 (CH_2, NCH_2CH_2), 13.2 (CH_3, ZnEt), 0.6 (CH_2, ZnEt).

Synthesis of 3a (white solid, 340 mg, yield: 83 %). **L3H** (1 equiv., 1.50 mmol, 267 mg) was dissolved in DCM (15 mL), and added to diethylzinc solution (1 equiv., 1 M in hexanes, 1.50 mmol, 1.50 mL). The mixture was stirred 2 h at rt. The volatiles were evaporated, and the residual solid was washed with pentane (2 x 5 mL) to give **3a**. **Elemental Analysis:** calcd for $C_{24}H_{36}N_4O_2Zn_2$: C, 53.05; H, 6.68; N, 10.31 %. Found: C, 52.66; H, 6.75; N, 10.02 %. **^{1}H NMR** (500 MHz, CD_2Cl_2): δ (ppm) = 7.49 (s, 2H, CH formamidine), 7.06 (pseudo td, $^3J_{HH}$ = 7.7 Hz, $^4J_{HH}$ = 1.9 Hz, 2H, Ar H_4), 6.98 (dd, $^3J_{HH}$ = 7.3 Hz, $^4J_{HH}$ = 1.8 Hz, 2H, Ar H_6), 6.65 (d, $^3J_{HH}$ = 8.0 Hz, 2H, Ar H_3), 6.60 (pseudo t, $^3J_{HH}$ = 7.2 Hz, 2H, Ar H_5), 4.45 (broad, 4H, $ArCH_2$), 3.05 (s, 12H, NMe_2), 0.87 (t, $^3J_{HH}$ = 8.1 Hz, 6H, CH_2CH_3), -0.16 (q, $^3J_{HH}$ = 8.0 Hz, 4H, CH_2CH_3). **^{13}C{^{1}H} NMR** (126 MHz, CD_2Cl_2): δ (ppm) = 163.6 (C_q, Ar C–O), 158.5 (C_q, C=N), 129.8 (C_q, Ar C_1), 129.2 (CH, Ar C_4), 128.8 (CH, Ar C_6), 120.1 (CH, Ar C_3), 116.7 (CH, Ar C_5), 59.8 (CH_2), 39.1 (bs, CH_3, NMe_2), 12.8 (CH_3, ZnEt), 0.1 (CH_2, ZnEt).

Synthesis of 4a (white solid, 366 mg, yield: 86 %). **L4H** (1 equiv., 1.50 mmol, 288 mg) was dissolved in DCM (15 mL), and added to diethylzinc solution (1 equiv., 1 M in hexane, 1.50 mmol, 1.50 mL). The mixture was stirred 2 h at rt. The volatiles were evaporated, and the residual solid was washed with pentane (2 x 5 mL) to give **4a** as a white solid. **Elemental Analysis:** calcd for $C_{26}H_{40}N_4O_2Zn_2$: C, 54.65; H, 7.06; N, 9.81 %. Found: C, 54.57; H, 7.16; N, 9.71 %. **^{1}H NMR** (500 MHz, CD_2Cl_2): δ (ppm) = 7.04 (pseudo t, $^3J_{HH}$ = 8.3 Hz, 2H, Ar H_4), 7.02 (d, $^3J_{HH}$ = 8.3 Hz, 2H, Ar H_6 overlapping with Ar H_4), 6.64 (d, $^3J_{HH}$ = 8.0 Hz, 2H, Ar H_3), 6.59 (pseudo t, $^3J_{HH}$ = 7.3 Hz, 2H, Ar H_5), 4.39 (s, 4H, $ArCH_2$), 3.08 (s, 12H, NMe_2), 2.08 (s, 6H, CH_3 acetamidine), 0.90 (t, $^3J_{HH}$ = 8.3 Hz, 6H, CH_2CH_3), -0.16 (q, $^3J_{HH}$ = 8.3 Hz, 4H, $CH_2CH_2CH_3$). **^{13}C{^{1}H} NMR** (126 MHz, CD_2Cl_2): δ (ppm) = 166.9 (C_q, C=N), 163.9 (C_q, Ar C–O), 129.7 (C_q, Ar C_1), 129.3 (CH, Ar $C_{4/6}$), 128.9 (CH, Ar $C_{4/6}$), 120.1 (CH, Ar C_3), 116.3 (CH, Ar C_5), 52.9 (CH_2, $ArCH_2$), 40.0 (CH_3, NMe_2), 15.5 (CH_3, acetamidine), 12.9 (CH_3, ZnEt), -0.4 (CH_2, ZnEt).

Synthesis of 1a' (white crystals, 75 mg, yield: 35 %). $ZnCl_2$ (1 equiv., 0.375 mmol, 53 mg) was suspended in THF (7.5 mL) and cooled to -80°C. In another Schlenk flask, phenate **L1Na** (2 equiv., 0.750 mmol, 207 mg) was solubilized in THF (15 mL), cooled to -80°C and slowly added to $ZnCl_2$. After addition, the -80°C bath was removed and the mixture stirred for 1 h at rt. Stirring was stopped and a resulting white salt was let to settle. The supernatant was cannulated with a borosilicate filter. The filtrate was concentrated to give the crude product as a white foam. It was further purified by vapor diffusion recrystallization using a toluene/pentane system to give the **1a'**. **HRMS (ESI-pos):** calcd for $[C_{32}H_{35}N_4O_2Zn]^+$ $[M + H]^+$: 571.20460. Found: 571.20325 (-2.4 ppm). **Elemental Analysis:** calcd for $C_{32}H_{34}N_4O_2Zn$: C, 67.19; H, 5.99; N, 9.79 %. Found: C, 66.32; H, 5.68; N, 9.46 %. **^{1}H NMR** (300 MHz, CD_2Cl_2): δ (ppm) = 7.61-7.50 (m, 4H + 2H, *m*-Ph and *p*-Ph), 7.36 (m, 2H, *o*-Ph), 7.06 (m, 2H, *o*-Ph), 7.01 (ddd, $^3J_{HH}$ = 8.1, 6.6 Hz, $^4J_{HH}$ = 2.5 Hz, 2H, Ar H_4), 6.62 (dd, $^3J_{HH}$ = 8.0 Hz, $^4J_{HH}$ = 1.1 Hz, 2H, Ar H_3), 6.33-6.27 (m, 2H + 2H, Ar H_6 and Ar H_5), 4.31 (d, $^2J_{HH}$ = 13.4 Hz, 2H, $ArCH_2$ AB spin system), 3.91 (d, $^2J_{HH}$ = 13.4 Hz, 2H, $ArCH_2$ AB spin system), 2.84 (s, 12H, NMe_2). **^{13}C{^{1}H} NMR** (126 MHz, CD_2Cl_2): δ (ppm) = 169.2 (C_q, C=N), 167.5 (C_q, Ar C–O), 133.4 (C_q, *i*-Ph), 130.7 (CH, *p*-Ph), 129.7 (CH, *m*-Ph , 129.5 (CH, Ar C_4), 129.4 (CH, Ar C_6), 129.3 (CH, *m*-Ph), 129.1 (CH, *o*-Ph), 128.4 (CH, *o*-Ph), 127.6 (C_q, Ar C_1), 119.6 (CH, Ar C_3), 113.6 (CH, Ar C_5), 55.7 (CH_2, $ArCH_2$), 40.1 (CH_3, NMe_2).

Synthesis of 1b (yellow powder, 240 mg, yield: 77%). THF solution (20 mL) of **L1H** (1 equiv., 1.00 mmol, 254 mg) was slowly added to a Schlenk flask containing trimethylaluminium solution (1 equiv., 2 M in

hexanes, 1.00 mmol, 0.500 mL). The mixture was stirred 2 h at rt. The volatiles were evaporated, and the residual solid was washed with pentane (3 x 10 mL) to give **1b**. Suitable crystal of **1b** for X-ray diffraction was obtained by vapor diffusion using a DCM/pentane system. **HRMS (ESI-pos):** calcd for $[C_{17}H_{20}AlN_2O]^+$ $[M - CH_3]^+$: 295.13855. Found: 295.13889 (-1.1 ppm). **Elemental Analysis:** calcd for $C_{18}H_{23}AlN_2O$: C, 69.66; H, 7.47; N, 9.03 %. Found: C, 69.71; H, 7.58; N, 9.37 %. **^{1}H NMR** (500 MHz, THF-d_8): δ (ppm) = 7.57 (m, 1H, *p*-Ph), 7.45 (m, 2H, *m*-Ph), 7.11 (m, 2H, *o*-Ph), 6.96 (pseudo td, $^3J_{HH}$ = 7.8 Hz, $^4J_{HH}$ = 1.8 Hz, 1H, Ar H_4), 6.60 (dd, $^3J_{HH}$ = 7.9 Hz, $^4J_{HH}$ = 1.2 Hz, 1H, Ar H_3), 6.34 (pseudo td, $^3J_{HH}$ = 7.4 Hz, $^4J_{HH}$ = 1.2 Hz, 1H, Ar H_5), 6.05 (dd, $^3J_{HH}$ = 7.4 Hz, $^4J_{HH}$ = 1.8 Hz, 1H, Ar H_6), 3.93 (s, 2H, $ArCH_2$), 3.03 (s, 6H, NMe_2), -0.80 (s, 6H, $AlMe_2$). **^{13}C{^{1}H} NMR** (126 MHz, THF-d_8): δ (ppm) = 173.3 (C_q, C=N), 162.0 (C_q, Ar C–O), 132.9 (C_q, *i*-Ph), 131.8 (CH, *p*-Ph), 129.7 (CH, *m*-Ph), 129.6 (CH, *o*-Ph), 129.4 (CH, Ar C_4), 128.8 (C_q, Ar C_1), 127.9 (CH, Ar C_6), 119.2 (CH, Ar C_3), 116.1 (CH, Ar C_5), 53.6 (CH_2, Ar*C*H_2), 41.5 (CH_3, NMe_2), -8.9 (broad, CH_3, $AlMe_2$).

Synthesis of 2b (white powder, 119 mg, yield: 75 %). Same procedure than for **1b**. **Elemental analysis:** calcd for $[C_{20}H_{25}AlN_2O]$: C, 71.41; H, 7.49; N, 8.33 %. Found: C, 70.60; H, 7.41; N, 7.80 %. **^{1}H NMR** (600 MHz, CD_2Cl_2,), δ (ppm): 7.56 (m, 1H, *p*-Ph), 7.49 (m, 2H, *m*-Ph), 7.08 (m, 2H, *o*-Ph overlapping with Ar H_4), 7.06 (pseudo t, $^3J_{H-H}$ = 7.9 Hz, 1H, Ar H_4), 6.70 (d, $^3J_{H-H}$ = 7.9 Hz, 1H, Ar H_3), 6.46 (pseudo t, $^3J_{H-H}$ = 7.2 Hz, 1H, Ar H_5), 6.11 (d, $^3J_{H-H}$ = 7.2 Hz, 1H, Ar H_6), 3.97 (s, 2H, $ArCH_2$), 3.45 (broad, 4H, 2 NCH_2CH_2), 1.91 (broad, 4H, NCH_2CH_2), -0.76 (s, 6H, CH_3). **^{13}C{^{1}H} NMR** (151 MHz, CD_2Cl_2), δ (ppm): 169.6 (C_q, C=N), 161.3 (C_q, Ar C–O), 133.3 (C_q, *i*-Ph), 130.9 (CH, *p*-Ph), 129.6 (CH, *m*-Ph), 129.4 (CH, Ar C_4), 128.9 (C_q, Ar C_1), 128.1 (CH, *o*-Ph), 127.9 (CH, Ar C_6), 118.7 (CH, Ar C_3), 116.6 (CH, Ar C_5), 52.8 (CH_2, Ar*C*H_2), 51.6 (CH_2, N*C*H_2CH_2), 25.6 (CH_2, NCH_2CH_2), -8.8 (broad, CH_3, $AlMe_2$).

Synthesis of 3b (beige solid, 320 mg, yield: 76 %). **L3H** (1 equiv., 1.80 mmol, 321 mg) was dissolved in DCM (9 mL), and added to trimethylaluminium solution (1 equiv., 2 M in hexanes, 1.80 mmol, 900 µL). The mixture was stirred 2 h at rt. The volatiles were evaporated, and the residual solid was washed with pentane (2 x 5 mL) to give **3b**. **Elemental Analysis:** calcd for $C_{12}H_{19}AlN_2O$: C, 61.52; H, 8.17; N, 11.96 %. Found: C, 60.81; H, 8.10; N, 11.28 %. **^{1}H NMR** (500 MHz, CD_2Cl_2): δ (ppm) = 7.44 (s, 1H, CH formamidine), 7.15 (pseudo td, $^3J_{HH}$ = 7.7 Hz, $^4J_{HH}$ = 1.8 Hz, 1H, Ar H_4), 7.02 (dd, $^3J_{HH}$ = 7.3 Hz, $^4J_{HH}$ = 1.8 Hz, 1H, Ar H_6), 6.75 (d, $^3J_{HH}$ = 8.0 Hz, 1H, Ar H_3), 6.66 (pseudo t, $^3J_{HH}$ = 7.4 Hz, 1H, Ar H_5), 4.30 (s, 2H, $ArCH_2$), 3.05 (s, 6H, NMe_2), -0.81 (s, 6H, $AlMe_2$). **^{13}C{^{1}H} NMR** (126 MHz, CD_2Cl_2): δ (ppm) = 160.7 (C_q, Ar C–O overlapping with C=N), 160.5 (broad, C_q, C=N overlapping with Ar C–O), 130.0 (CH, Ar C_4), 128.4 (C_q, Ar C_1), 127.6 (CH, Ar C_6), 119.2 (CH, Ar C_3), 117.3 (CH, Ar C_5), 58.2 (CH_2, Ar*C*H_2), 42.2 (broad, CH_3, NMe overlapping with NMe), 39.3 (broad, CH_3, NMe overlapping with NMe), -8.1 (broad, CH_3, $AlMe_2$).

Synthesis of 4b (beige powder, 320 mg, yield: 85 %). Same procedure than for **3b**. **Elemental Analysis:** calcd for $C_{13}H_{21}AlN_2O$: C, 62.88; H, 8.52; N, 11.28 %. Found: C, 62.05; H, 8.47; N, 10.36 %. **HRMS (ESI-pos):** calcd for $[C_{13}H_{22}AlN_2O]^+$ $[M + H]^+$: 249.15420. Found: 249.15355 (-2.6 ppm)**. ^{1}H NMR** (500 MHz, CD_2Cl_2): δ (ppm) = 7.11 (pseudo td, $^3J_{HH}$ = 7.7 Hz, $^4J_{HH}$ = 1.8 Hz, 1H, Ar H_4), 7.04 (dd, $^3J_{HH}$ = 7.3 Hz, $^4J_{HH}$ = 1.8 Hz, 1H, Ar H_6), 6.69 (d, $^3J_{HH}$ = 8.0 Hz, 1H, Ar H_3), 6.63 (pseudo t, $^3J_{HH}$ = 7.3 Hz, 1H, Ar H_5), 4.23 (s, 2H, $ArCH_2$), 3.09 (s, 6H, NMe_2), 2.17 (s, 3H, CH_3 acetamidine), -0.86 (s, 6H, $AlMe_2$). **^{13}C{^{1}H} NMR** (126 MHz, CD_2Cl_2): δ (ppm) = 171.6 (C_q, C=N), 161.3 (C_q, Ar C–O), 129.7 (CH, Ar C_4), 128.4 (C_q, Ar C_1), 127.6 (CH, Ar C_6), 119.0 (CH, Ar C_3), 116.7 (CH, Ar C_5), 51.2 (CH_2, Ar*C*H_2), 41.3 (CH_3, NMe_2), 16.7 (CH_3, acetamidine), -9.5 (broad, CH_3, $AlMe_2$).

ASSOCIATED CONTENT

Supporting Information

The Supporting Information is available free of charge on the ACS Publications website.

NMR spectra of compounds **L1H-L4H**, **[L1H$_2$][Br], L1Na, 1a-4a**, **1a'** and **1b-4b**. ^{1}H NMR monitoring of the evolution of **L1H** into 2-Phenyl-4H-1,3-benzoxazine.

Tables of crystal data for the proligands **[L1H$_2$][Br]** , **L2H** and for the complexes **1a**, **2a**, **1a'**, **1a", 1b** and **2b**.

Graph of the PLA M_n values as a function of lactide conversion, Graph of $\ln([M]_0/[M])$ versus time, GPC analysis, MALDI-TOF spectra.

Accession Codes

CCDC 1868743, 1868745-1868750 and 1937786 contain the Supporting crystallographic data for this paper. These data can be obtained free of charge via www.ccdc.cam.ac.uk/data_request/cif, or by emailing data request@ccdc.cam.ac.uk, or by contacting The Cambridge Crystallographic Data Centre, 12 Union Road, Cambridge CB2 1EZ, UK; fax: +44 1223 336033.

AUTHOR INFORMATION

Corresponding Authors

* E-mail: dagorne@unistra.fr, Tel: +33 (0)3 68 85 15 30; pierre.le-gendre@u-bourgogne.fr, Tel: +33 (0)3 80 39 60 82;

Notes

The authors declare no competing financial interest.

ACKNOWLEDGMENTS

Support was provided by the Ministère de l'Enseignement Supérieur et de la Recherche, and the Centre National de la Recherche Scientifique (CNRS). This work is part of the project CHIMIE DURABLE, ENVIRONNEMENT ET AGROALIMENTAIRE, supported by the Université de Bourgogne, Conseil Régional de Bourgogne through the plan d'actions régional pour l'innovation (PARI) and the European Union through the PO FEDER-FSE Bourgogne 2014/2020 programs.

REFERENCES

(1) Phenoxyimine metal complexes for olefin polymerization, for a review see: (a) Makio, H.; Terao, H.; Iwashita, A.; Fujita, T. FI Catalysts for Olefin Polymerization—A Comprehensive Treatment. *Chem. Rev.* **2011**, *111*, 2363-2449. For representative examples see: (b) Saito, J.; Mitani, M.; Matsui, S.; Sugi, M.; Tohi, Y.; Tsutsui, T.; Fujita, T.; Nitabaru, M.; Makio, H. (Mitsui Chemicals). Olefin polymerization catalysts, transition metal compounds, processes for olefin polymerization, and Alpha-olefin/conjugated diene copolymers, European Patent Application EP-0874005, 1997. (c) Johnson, L. K.; Bennett, A. M.; Ittel, S. D.; Wang, L.; Parthasarathy, A.; Hauptman, E.; Simpson, R. D.; Feldman, J.; Coughlin, E. B. (Du Pont De Nemours and Company). Polymerisation of olefins. WO Patent 9830609, 1998. (d) Bansleben, D. A.; Friedriich, S. K.; Younkin, T. D.; Grubbs, R. H.; Wang, C.; Li, R. T. (W.R. Grace & Co.-Conn.). Catalysts compositions and processes for polymers and copolymers. WO Patent 9842664, 1998. (e) Wang, C.; Friedrich, S.; Younkin, T. R.; Li, R. T.; Grubbs, R. H.; Bansleben, D. A.; Day, M. W. Neutral Nickel(II)-Based Catalysts for Ethylene Polymerization. *Organometallics* **1998**, *17*, 3149-3151. (f) Younkin, T. R.; Connor, E. F.; Henderson, J. I.; Friedrich, S. K.; Grubbs, R. H.; Bansleben, D. A. Neutral, Single-Component Nickel (II) Polyolefin Catalysts That Tolerate Heteroatoms. *Science* **2000**, *287*, 460-462. (g) Cai, Z.; Xiao, D.; Do, L. H. Fine-Tuning Nickel Phenoxyimine Olefin Polymerization Catalysts: Performance Boosting by Alkali Cations. *J. Am. Chem. Soc.* **2015**, *137*, 15501-15510. (h) Gao, Y.; Christianson, M. D.; Wang, Y.; Chen, J.; Marshall, S.; Klosin, J.; Lohr, T. L.; Marks, T. J. Unexpected Precatalyst sigma-Ligand Effects in Phenoxyimine Zr-Catalyzed Ethylene/1-Octene Copolymerizations. *J. Am. Chem. Soc.* **2019**, *141*, 7822-7830.

(2) For representative examples of phenoxyimine metal complexes for ROP of cyclic esters, see: (a) Nomura, N.; Aoyama, T.; Ishii, R.; Kondo, T. Salicylaldimine–Aluminum Complexes for the Facile and Efficient Ring-Opening Polymerization of ε-Caprolactone. *Macromolecules* **2005**, *38*, 5363-5366. (b) Chen, H.-Y.; Tang, H.-Y.; Lin, C.-C. Ring-Opening Polymerization of Lactides Initiated by Zinc Alkoxides Derived from NNO-Tridentate Ligands. *Macromolecules* **2006**, *39*, 3745-3752. (c) Liu, J.; Iwasa, N.; Nomura, K. Synthesis of Al complexes containing phenoxy-imine ligands and their use as the catalyst precursors for efficient living ring-opening polymerisation of ε-caprolactone. *Dalton Trans.* **2008**, 3978-3988. (d) Pappalardo, D.; Annunziata, L.; Pellecchia, C. Living Ring-Opening Homo- and Copolymerization of ε-Caprolactone and *L*- and *D*,*L*-Lactides by Dimethyl(salicylaldiminato)aluminum Compounds. *Macromolecules* **2009**, *42*, 6056-6062. (e) García-Valle, F. M.; Tabernero, V.; Cuenca, T.; Mosquera, M. E. G.; Cano, J.; Milione, S. Biodegradable PHB from rac-β-Butyrolactone: Highly Controlled ROP Mediated by a Pentacoordinated Aluminum Complex. *Organometallics* **2018**, *37*, 837-84.

(3) (a) Manna, K.; Zhang, T.; Carboni, M.; Abney, C. W.; Lin, W. Salicylaldimine-Based Metal–Organic Framework Enabling Highly Active Olefin Hydrogenation with Iron and Cobalt Catalysts. *J. Am. Chem. Soc.* **2014**, *136*, 13182-13185. (b) Jia, W.-G.; Zhang, H.; Zhang, T.; Xie, D.; Ling, S.; Sheng, E.-H. Half-Sandwich Ruthenium Complexes with Schiff-Base Ligands: Syntheses, Characterization, and Catalytic Activities for the Reduction of Nitroarenes. *Organometallics* **2016**, *35*, 503-512.

(4) Yang, H.-L.; Cai, P.; Liu, Q.-H.; Yang, X.-L.; Fang, S.-Q.; Tang, Y.-W.; Wang, C.; Wang, X.-B.; Kong, L.-Y. Design, synthesis, and evaluation of salicyladimine derivatives as multitarget-directed ligands against Alzheimer's disease. *Biorg. Med. Chem.* **2017**, *25*, 5917-5928.

(5) Hoshino, N. Liquid crystal properties of metal–salicylaldimine complexes: Chemical modifications towards lower symmetry. *Coord. Chem. Rev.* **1998**, *174*, 77-108.

(6) Chang, M.-C.; Lu, W.-Y.; Chang, H.-Y.; Lai, Y.-C.; Chiang, M. Y.; Chen, H.-Y.; Chen, H.-Y. Comparative Study of Aluminum Complexes Bearing N,O- and N,S-Schiff Base in Ring-Opening Polymerization of ε-Caprolactone and l-Lactide. *Inorg. Chem.* **2015**, *54*, 11292-11298.

(7) Liu, X.; Gao, W.; Mu, Y.; Li, G.; Ye, L.; Xia, H.; Ren, Y.; Feng, S. Dialkylaluminum Complexes with Chelating Anilido-Imine Ligands: Synthesis, Structures, and Luminescent Properties. *Organometallics* **2005**, *24*, 1614-1619.

(8) (a) Hogerheide, M. P.; Wesseling, M.; Jastrzebski, J. T. B. H.; Boersma, J.; Kooijman, H.; Spek, A. L.; van Koten, G. Versatility in Phenolate Bonding in Organoaluminum Complexes Containing Mono- and Bis-ortho-Chelating Phenolate Ligands. X-ray Structures of $Al\{OC_6H_2(CH_2NMe_2)_2\text{-}2,6\text{-}Me\text{-}4\}_3$, $Al(Me)_2\{OC_6H_2(CH_2NMe_2)_2\text{-}2,6\text{-}Me\text{-}4\}\cdot N\text{-}AlMe_3$, and $Al(Me)_2\{OC_6H_2(CH_2NMe_2)2\text{-}2,6\text{-}Me\text{-}4\}\cdot N\text{-}AlMe_3\cdot O\text{-}AlMe_3$ *Organometallics* **1995**, *14*, 4483-4492. (b) Dagorne, S.; Lavanant, L.; Chassenieux, C.; Haquette, P.; Jaouen, G. *Organometallics* **2003**, *22*, 3732-3741. (c) Dagorne, S.; Le Bideau F.; Welter, R.; Bellemin-Laponnaz, S.; Maisse-François, A. Well-Defined Cationic Alkyl– and Alkoxide–Aluminum Complexes and Their Reactivity with ε-Caprolactone and Lactides. *Chem. Eur. J.* **2007**, *13*, 3202-3217.

(9) Cheisson, T.; Cao, T.-P.-A.; Le Goff, X. F.; Auffrant, A. Nickel Complexes Featuring Iminophosphorane–Phenoxide Ligands for Catalytic Ethylene Dimerization. *Organometallics* **2014**, *33*, 6193-6199.

(10) (a) Waltman, A. W.; Grubbs, R. H. A New Class of Chelating N-Heterocyclic Carbene Ligands and Their Complexes with Palladium. *Organometallics* **2004**, *23*, 3105-3107. (b) Seok Oh, C.; Won Lee, C.; Yeob Lee, J. Simple heteroatom engineering for tuning the triplet energy of organometallic host materials for red, green and blue phosphorescent organic light-emitting diodes. *Chem. Commun.* **2013**, *49*, 3875-3877. (c) Zhang, Y.; Gao, A.; Zhang, Y.; Xu, Z.; Yao, W. Aluminum complexes with benzoxazolphenolate ligands: Synthesis, characterization and catalytic properties for ring-opening polymerization of cyclic esters. *Polyhedron* **2016**, *112*, 27-33. (d) Sarada, G.; Sim, B.; Cho, W.; Yoon, J.; Gal, Y.-S.; Kim, J.-J.; Jin, S.-H. New sky-blue and bluish–green emitting Ir(III) complexes containing an azoline ancillary ligand for highly efficient PhOLEDs. *Dyes and Pigments* **2016**, *131*, 60-68. (e) Li, M.; Shu, X.; Cai, Z.; Eisen, M. S. Synthesis, Structures, and Norbornene Polymerization Behavior of Neutral Nickel(II) and Palladium(II) Complexes Bearing Aryloxide Imidazolidin-2-imine Ligands. *Organometallics* **2018**, *37*, 1172-1180.

(11) Hegarty, A. F.; Chandler, A. Isomerisation about the C–N and C=N bonds of E- and Z-amidines. *J. Chem. Soc., Chem. Commun.* **1980**, 130-131.

(12) (a) Coles, M. P. Application of neutral amidines and guanidines in coordination chemistry. *Dalton Trans.* **2006**, 985-1001. (b) Panda, T. K.; Tsurugi, H.; Pal, K.; Kaneko, H.; Mashima, K. Highly Reactive Metal−Nitrogen Bond Induced C−H Bond Activation and Azametallacycle Formation. *Organometallics* **2010**, *29*, 34-37. (c) Rad'kov, V.; Roisnel T.; Trifonov A. ; Carpentier, J.-F.; Kirillov E. Neutral and Cationic Alkyl and Amido Group 3 Metal Complexes of Amidine-Amidopyridinate Ligands: Synthesis, Structure, and Polymerization Catalytic Activity. *Eur. J. Inorg. Chem.* **2014**, *2014*, 4168-4178. (d) Lapshin, I. V.; Yurova, O. S.; Basalov, I. V.; Rad'kov, V. Y.; Musina, E. I.; Cherkasov, A. V.; Fukin, G. K.; Karasik, A. A.;

Trifonov, A. A. Amido Ca and Yb(II) Complexes Coordinated by Amidine-Amidopyridinate Ligands for Catalytic Intermolecular Olefin Hydrophosphination. *Inorg. Chem.* **2018**, *57*, 2942-2952.

(13) For a review see: (a) Edelmann, F. T. Lanthanide amidinates and guanidinates: from laboratory curiosities to efficient homogeneous catalysts and precursors for rare-earth oxide thin films. *Chem. Soc. Rev.* **2009**, *38*, 2253-2268. For representative examples, see: (b) Stewart, P. J.; Blake, A. J.; Mountford, P. New Titanium Complexes Containing an Amidinate−Imide Supporting Ligand Set: Cyclopentadienyl, Alkyl, Borohydride, Aryloxide, and Amide Derivatives. *Organometallics* **1998**, *17*, 3271-3281. (c) Aharonovich, S.; Kapon, M.; Botoshanski, M.; Eisen, M. S. N,N′-Bis-Silylated Lithium Aryl Amidinates: Synthesis, Characterization, and the Gradual Transition of Coordination Mode from σ Toward π Originated by Crystal Packing Interactions. *Organometallics* **2008**, *27*, 1869-1877. (d) Weitershaus, K.; Ward, B. D.; Kubiak, R.; Müller, C.; Wadepohl, H.; Doye, S.; Gade, L. H. Titanium hydroamination catalysts bearing a 2-aminopyrrolinato spectator ligand: monitoring the individual reaction steps. *Dalton Trans.* **2009**, 4586-4602. (e) Hong, J.; Zhang, L.; Wang, K.; Chen, Z.; Wu, L.; Zhou, X. Synthesis, Structural Characterization, and Reactivity of Mono(amidinate) Rare-Earth-Metal Bis(aminobenzyl) Complexes. *Organometallics* **2013**, *32*, 7312-7322. (f) Collins, R. A.; Russell, A. F.; Scott, R. T. W.; Bernardo, R.; van Doremaele, G. H. J.; Berthoud, A.; Mountford, P. Monometallic and Bimetallic Titanium κ^1-Amidinate Complexes as Olefin Polymerization Catalysts. *Organometallics* **2017**, *36*, 2167-2181. (g) Wei, J.; Duman, L. M.; Redman, D. W.; Yonke, B. L.; Zavalij, P. Y.; Sita, L. R. N-Substituted Iminocaprolactams as Versatile and Low Cost Ligands in Group 4 Metal Initiators for the Living Coordinative Chain Transfer Polymerization of α-Olefins. *Organometallics* **2017**, *36*, 4202-4207. (h) Rios Yepes, Y.; Quintero, C.; Osorio Meléndez, D.; Daniliuc, C. G.; Martínez, J.; Rojas, R. S. Cyclic Carbonates from CO_2 and Epoxides Catalyzed by Tetra- and Pentacoordinate Amidinate Aluminum Complexes. *Organometallics* **2018**, *38*, 469-478.(i) Kaufmann, S.; Radius, M.; Moos, E.; Breher, F.; Roesky, P. W. Rhodium(I) and Iridium(I) Complexes of Ferrocenyl-Functionalized Amidinates and Bis(amidinates): κ^2N-Coordination Versus Ferrocenyl Ortho-Metalation. *Organometallics* **2019**, *38*, 1721-1732.

(14) (a) Sinenkov, M.; Kirillov, E.; Roisnel, T.; Fukin, G.; Trifonov, A.; Carpentier, J.-F. Rare-Earth Complexes with Multidentate Tethered Phenoxy-Amidinate Ligands: Synthesis, Structure, and Activity in Ring-Opening Polymerization of Lactide. *Organometallics* **2011**, *30*, 5509-5523. (b) Kirillov, E.; Roisnel, T.; Carpentier, J.-F. Synthesis and Structural Diversity of Group 4 Metal Complexes with Multidentate Tethered Phenoxy-Amidine and Phenoxy-Amidinate Ligands. *Organometallics* **2012**, *31*, 3228-3240.

(15) Representative reviews on metal-mediated lactide ROP catalysis: (a) O'Keefe, B. J.; Hillmyer, M. A.; Tolman, W. B. Polymerization of lactide and related cyclic esters by discrete metal complexes. *J. Chem. Soc., Dalton Trans.* **2001**, 2215-2224; (b) Dechy-Cabaret, O.; Martin-Vaca, B.; Bourissou, D. Controlled Ring-Opening Polymerization of Lactide and Glycolide. *Chem. Rev.* **2004**, *104*, 6147-6176; (c) Platel, R. H.; Hodgson, L. M.; Williams, C. K. Biocompatible Initiators for Lactide Polymerization. *Polym. Rev.* **2008**, *48*, 11-63; (d) Thomas, C. M. Stereocontrolled ring-opening polymerization of cyclic esters: synthesis of new polyester microstructures. *Chem. Soc. Rev.* **2010**, *39*, 165-173; (e) Stanford, M. J.; Dove, A. P. Stereocontrolled ring-opening polymerisation of lactide. *Chem. Soc. Rev.* **2010**, *39*, 486-494; (f) Buffet, J.-C.; Okuda, J. Initiators for the stereoselective ring-opening polymerization of meso-lactide. *Polym. Chem.* **2011**, *2*, 2758-2763; (g) Sauer, A.; Kapelski, A.; Fliedel, C.; Dagorne, S.; Kol, M.; Okuda, J. Structurally well-defined group 4 metal complexes as initiators for the ring-opening polymerization of lactide monomers. *Dalton Trans.* **2013**, *42*, 9007-9023; (h) Dagorne, S.; Normand, M.; Kirillov, E.; Carpentier, J.-F. Gallium and indium complexes for ring-opening polymerization of cyclic ethers, esters and carbonates. *Coord. Chem. Rev.* **2013**, *257*, 1869-1886; (i) Guillaume, S. M.; Kirillov, E.; Sarazin, Y.; Carpentier, J.-F. Beyond Stereoselectivity, Switchable Catalysis: Some of the Last Frontier Challenges in Ring-Opening Polymerization of Cyclic Esters. *Chem. Eur. J.* **2015**, *21*, 7988-8003. (j) Le Roux, E. Recent advances on tailor-made titanium catalysts for biopolymer synthesis. *Coord. Chem. Rev.* **2016**, *306, Part 1*, 65-85.

(16) (a) Dunn, P. J.: 5.19 - Amidines and N-Substituted Amidines. In *Comprehensive Organic Functional Group Transformations II*; Katritzky, A. R., Taylor, R. J. K., Eds.; Elsevier: Oxford, 2005; pp 655-699. (b) Aly, A. A.; Nour-El-Din, A. M. Functionality of amidines and amidrazones, *Arkivoc* **2008**, (i), 153-194.

(17) Toste, D.; McNulty, J.; Still, I. W. J. Formamidine as a Versatile Protecting Group for Primary Amines: A Mild Procedure for Hydrolytic Removal. *Synth. Commun.* **1994**, *24*, 1617-1624.

(18) Comparison between the NMe_2 signal profiles in the ^1H NMR spectra of **L1H**, **L3H** and **L4H** should be taken with caution since the spectra have not been registered in the same conditions (deuterated solvent, NMR magnetic field).

(19) Rotational barrier was calculated from the dynamic exchange between Hα protons. Rotational barriers of 61.6(5) kJ mol^{-1} and 52.2(5) kJ mol^{-1} were calculated from the dynamic exchange between Hβ protons of the pyrrolidine ring in the proligand **L2H** and in the complex **2b**, respectively. ^1H NMR spectra were recorded every 5 K. The coalescence temperatures were chosen at the center of the interval where coalescence occurred. To determine the uncertainties due to the temperature we suppose an uniform distribution over the 5 K interval. The uncertainty due to the frequencies are negligible. As usual, expanded uncertainties are given at the 95% confidence level.

(20) McKennis, J. S.; Smith, P. A. S. Restricted rotation in benzamidinium systems. *J. Org. Chem.* **1972**, *37*, 4173-4178.

(21) Wawer, I. Hindered rotation in amidines. *J. Mol. Struct.* **1990**, *218*, 165-167.

(22) Oszczapowicz, J.; Wawer, I.; Dargatz, M.; Kleinpeter, E. Amidines. Part 34.^{15}N NMR spectra of trisubstituted amidines. Substituent effects. *J. Chem. Soc., Perkin Trans. 2* **1995**, 1127-1131.

(23) Rotational barrier of 56.6(5) kJ mol^{-1} was calculated from the dynamic exchange between Hα protons of the ethyl ligand in **1a**.

(24) The dissociation of the dinuclear complex **1a** into the mononuclear form decreased the steric constraints around the phenoxyamidine ligand enabling faster flipping motion of the metallacycle and the non-persistence of the sp^2-sp^3 atropoisomeric chirality in the monomer even at low temperature. Therefore, no diastereotopic splitting of the methylene protons is observed for the monomer.

(25) Bouyhayi, M.; Sarazin, Y.; Casagrande Jr, O. L.; Carpentier, J.-F. Aluminum, calcium and zinc complexes supported by potentially tridentate iminophenolate ligands: synthesis and use in the ring-opening polymerization of lactide. *Appl. Organomet. Chem.* **2012**, *26*, 681-688.

(26) An analogous spiro Zinc complex with phenoxyimine ligands has been previously described, see: Chisholm, M. H.; Gallucci, J. C.; Zhen, H.; Huffman, J. C. Three-Coordinate Zinc Amide and Phenoxide Complexes Supported by a Bulky Schiff Base Ligand. *Inorg. Chem.* **2001**, *40*, 5051-5054.

(27) For a review see: (a) Wheaton, C. A.; Hayes, P. G.; Ireland, B. J. Complexes of Mg, Ca and Zn as homogeneous catalysts for lactide polymerization. *Dalton Trans.* **2009**, 4832-4846. For representative examples, see: (b) Chamberlain, B. M.; Cheng, M.; Moore, D. R.; Ovitt, T. M.; Lobkovsky, E. B.; Coates, G. W. Polymerization of Lactide with Zinc and Magnesium β-Diiminate Complexes: Stereocontrol and Mechanism. *J. Am. Chem. Soc.* **2001**, *123*, 3229-3238. (c) Williams, C. K.; Breyfogle, L. E.; Choi, S. K.; Nam, W.; Young, V. G.; Hillmyer, M. A.; Tolman, W. B. A Highly Active Zinc Catalyst for the Controlled Polymerization of Lactide. *J. Am. Chem. Soc.* **2003**, *125*, 11350-11359. (d) Yu, X.-F.; Zhang, C.; Wang, Z.-X. Rapid and Controlled Polymerization of rac-Lactide Using N,N,O-Chelate Zinc Enolate Catalysts. *Organometallics* **2013**, *32*, 3262-3268; (e) Kan, C.; Hu, J.; Huang, Y.; Wang, H.; Ma, H. Highly Isoselective and Active Zinc Catalysts for rac-Lactide Polymerization: Effect of Pendant Groups of Aminophenolate Ligands. *Macromolecules* **2017**, *50*, 7911-7919.

(28) Hung, W.-C.; Huang, Y.; Lin, C.-C. Efficient initiators for the ring-opening polymerization of L-lactide: Synthesis and characterization of NNO-tridentate Schiff-base zinc complexes. *J. Polym. Sci., Part A: Polym. Chem.* **2008**, *46*, 6466-6476.

(29) Normand, M.; Dorcet, V.; Kirillov, E.; Carpentier, J.-F. {Phenoxy-imine}aluminum versus -indium Complexes for the Immortal ROP of Lactide: Different Stereocontrol, Different Mechanisms. *Organometallics* **2013**, *32*, 1694-1709.

(30) Iwasa, N.; Fujiki, M.; Nomura, K. Ring-opening polymerization of various cyclic esters by Al complex catalysts containing a series of phenoxy-imine ligands: Effect of the imino substituents for the catalytic activity. *J. Mol. Catal. A: Chem.* **2008**, *292*, 67-75.

(31) Zhang, W.; Wang, Y.; Sun, W.-H.; Wang, L.; Redshaw, C. Dimethylaluminium aldiminophenolates: synthesis, characterization and ring-opening polymerization behavior towards lactides. *Dalton Trans.* **2012**, *41*, 11587-11596.

(32) Dagorne, S.; Fliedel C. Organoaluminum Species in Homogeneous Polymerization Catalysis. *Top. Organomet. Chem*., **2013**, *41*, 125-172.

(33) Zelli, R.; Zeinyeh, W.; Haudecoeur, R.; Alliot, J.; Boucherle, B.; Callebaut, I.; Décout, J.-L. A One-Pot Synthesis of Highly Functionalized Purines. *Org. Lett.* **2017**, *19*, 6360-6363.

(34) Dolomanov, O. V.; Bourhis, L. J.; Gildea, R. J.; Howard, J. A. K.; Puschmann, H. OLEX2: a complete structure solution, refinement and analysis program. *J. Appl. Crystallogr.* **2009**, *42*, 339-341.

(35) Sheldrick, G. SHELXT - Integrated space-group and crystal-structure determination. *Acta Crystallographica Section A* **2015**, *71*, 3-8.

(36) Sheldrick, G. SHELXL – Crystal structure refinement with SHELXL. *Acta Crystallographica Section C* **2015**, *71*, 3-8.

TOC Graphic

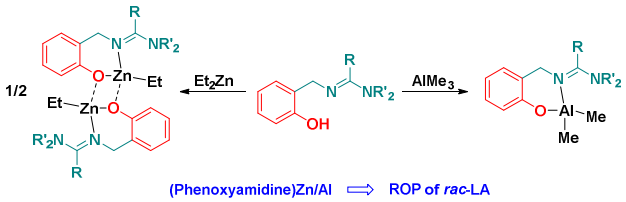

(Phenoxyamidine)Zn/Al ⟹ ROP of *rac*-LA